AN ABSTRACT OF THE THESIS OF

Alson R. Kemp III for the degree of Master of Science in Electrical and Computer Engineering presented on June 13, 1996.

Title: Use of Multiple Loop Model for Brushless Doubly Fed Machine Rotor Design

Redacted for Privacy

Abstract approved: _____

Alan Wallace

The Brushless Doubly Fed Machine (BDFM) is receiving attention as a candidate for use in adjustable speed drives (ASDs) and variable speed generators (VSGs). With a large percentage of a drive or generator system's cost due to power electronics content, considerable research has been conducted to find drives in which the power electronics can be minimized. Generally, the power electronics in a drive must be able to process the full apparent power rating of the machine. With the BDFM, the power electronics must only process a fraction of the apparent power rating of the machine, and so can be less expensive than alternative solutions.

Rotor designs for the BDFM have assumed that the currents in the rotor bars are evenly distributed and have used equal area rotor bars. Qualitative observation suggested that rotor currents are not distributed equally between the rotor bars. Test data and novel simulation methods were used to quantitatively assess the current distributions in the rotor bars.

Rotor current distributions can be investigated three ways: finite element analysis, test data from a modified BDFM, and simulation using a novel multiple rotor circuit model. The latter two methods were employed to obtain the results presented in this thesis. The multiple loop model of the BDFM is presented and use of the model is described. To demonstrate the capabilities of the model, designs for two different applications is presented.

©Copyright by Alson R. Kemp III

June 13, 1996

All Rights Reserved

Use of Multiple Loop Model for Brushless Doubly Fed Machine Rotor Design

by

Alson R. Kemp III

A THESIS

submitted to

Oregon State University

in partial fulfillment of the

requirements for the degree of

Master of Science

Completed June 13, 1996

Commencement June 1997

Master of Science thesis of Alson R. Kemp III presented on June 13, 1996

APPROVED:

Redacted for Privacy

Redacted for Privacy

Major Professor, representing Electrical and Computer Engineering

Redacted for Privacy

Head of Department of Electrical and Computer Engineering

Redacted for Privacy

Dean of Graduate School

I understand that my thesis will become part of the permanent collection of Oregon State University libraries. My signature below authorizes release of my thesis to any reader upon request.

Redacted for Privacy

Alson R. Kemp III, Author

ACKNOWLEDGEMENTS

Thanks to Dr. Alan Wallace for guiding me through graduate school, trusting me with BDFM research and being great to work with. Thanks to Dr. Rene Spee for providing me with machine design experience, ideas and education.

Thanks to my family, without whom none of this would be possible.

This research was funded by Bonneville Power Administration, Electrical Power Research Institute and Puget Sound Power and Light.

TABLE OF CONTENTS

		Page
1	Introduction	1
2	Description of BDFM	3
2.1	General Description	3
2.2	Stator Structure	5
2.3	Rotor Structure	6
3	Multiple Loop Model	8
3.1	Background	8
3.2	Development of the Model	9
3.2.1	Dynamic Model	11
3.2.2	Steady-State Model	13
3.3	Sample Model Parameters	14
3.4	Model Implentation	16
3.5	Design Programs	19
3.5.1	*mlspeedmot*	19
3.5.2	*mlspeedgen*	21
4	Verification of the Model	23
4.1	Finite Element Analysis	23
4.1.1	Simplification of the Finite Element Analysis	24
4.1.2	Comparison to the Multiple Loop Model	24
4.2	Experimental Verification	24
4.2.1	Experimental Procedure	26
4.2.2	Comparison to the Multiple Loop Model	27
5	$5Hp$ Demonstration Drive	29
5.1	The Two Design Approaches	30

TABLE OF CONTENTS (CONTINUED)

		Page
5.2	Stator Design	33
5.3	Rotor Design	34
5.4	Cost Estimate	39
6	200kW Stand-alone Aircraft Generator	41
6.1	Summary of Aircraft Power Generation	41
6.2	BDFM Design Alternatives	43
6.3	Proposed Design	46
6.4	Cost Estimate	47
7	Design Conclusion	50
8	Conclusions	52
Bibliography		54
Appendix		56

LIST OF FIGURES

Figure		Page
1.1.	BDFM System Diagram	2
2.1.	BDFM Rotor Structures	6
3.1.	Single Loop Model Circuit	9
3.2.	Multiple Loop Model Circuit	10
3.3.	Diagram of Rotor Nest with 4 Loops	15
3.4.	MLM Program Hierarchy	17
3.5.	Power Flow for BDFM Generator	21
4.1.	Comparison of Finite Element Analysis and Multiple Loop Model	25
4.2.	Experimental Measurements of Rotor Loop Currents	27
4.3.	Comparison of Test Results with Multiple Loop Model	28
5.1.	Square Pole Machine : Converter Rating : Pump Load	30
5.2.	"NEMA" Design : Converter Rating : Pump Load	31
5.3.	Square Pole Design : Machine Efficiency : Pump Load	31
5.4.	"NEMA" Design : Machine Efficiency : Pump Load	32
5.5.	Stator Tooth Flux Densities	35
5.6.	Rotor Current Induced MMF for $3\frac{Loops}{Nest}$	35
5.7.	Rotor Current Induced MMF for $4\frac{Loops}{Nest}$	36
5.8.	Rotor Currents : $600 \rightarrow 900\frac{r}{min}$: Pump Load	38
5.9.	Rotor Bar Diagram	38
6.1.	3-1 Machine : Converter Rating	44
6.2.	4-2 Machine : Converter Rating	45
6.3.	3-1 BDFM Design Tooth Flux Densities	47
6.4.	4-2 BDFM Design Tooth Flux Densities	48

LIST OF TABLES

Table		Page
1.	Experimental Machine Description	26
2.	Comparison of Two 5hp Design Dimensions	32
3.	Proposed Design Stator Description	33
4.	Proposed Design Rotor Description	37
5.	Current Distributions in Rotor Bars and Bar Sizes at $900\frac{r}{min}$	39
6.	Cost Estimate	40
7.	Specification for Aircraft Power Generation System	42
8.	Comparison of Two $200kW$ Design Dimensions	43
9.	Comparison of Two 200kW Design Performances	44
10.	Current Distributions in Rotor Bars and Bar Sizes	48
11.	Cost Estimate	49

LIST OF SYMBOLS

f_c	Control winding excitation frequency
f_p	Power winding excitation frequency
f_r	Rotor current electrical frequency
f_R	Rotor mechanical frequency
I_c	RMS control winding current
i_{0c}	Control winding 0-sequence current
i_{dc}	Control winding d-sequence current
i_{qc}	Control winding q-sequence current
I_p	RMS power winding current
i_{0p}	Power winding 0-sequence current
i_{dp}	Power winding d-sequence current
i_{qp}	Power winding q-sequence current
$\mathbf{I_r}$	RMS rotor current matrix
i_{drcx}	Rotor loop x d-sequence current from coupling to the control winding
i_{qrcx}	Rotor loop x q-sequence current from coupling to the control winding
i_{drpx}	Rotor loop x d-sequence current from coupling to the power winding
i_{qrpx}	Rotor loop x q-sequence current from coupling to the power winding
I_{rx}	RMS rotor current for loop x
L_{lc}	Control winding leakage inductance
$L_{l-endring}$	Leakage inductance of common section of endring.
L_{lp}	Power winding leakage inductance
$\mathbf{L_{lr}}$	Rotor leakage inductance matrix
L_{lrxx}	Leakage inductance of rotor loop x
L_{lrxy}	Endring section leakage inductance affecting voltage around loop x and affected by current in rotor loop y

L_{mc}	Control winding magnetizing inductance
L_{mp}	Power winding magnetizing inductance
m	Number of loops per rotor nest
$\mathbf{M_{cr}}$	Control winding to rotor mutual inductance matrix
M_{crx}	Control winding to rotor loop x mutual inductance
$\mathbf{M_{pr}}$	Power winding to rotor mutual inductance matrix
M_{prx}	Power winding to rotor loop x mutual inductance
P_c	Control winding pole pairs
P_p	Power winding pole pairs
P_r	Rotor poles or rotor nests
R_c	Control winding resistance
$R_{endring}$	Resistance of common section of endring.
R_p	Power winding resistance
$\mathbf{R_r}$	Rotor resistance matrix
R_{rxx}	Resistance of rotor loop x
R_{rxy}	Endring section resistance affecting voltage around loop x and affected by current in rotor loop y
T_l	Load torque on the rotor shaft
TPC_c	Control winding turns per coil
TPC_p	Power winding turns per coil
v_{0c}	Control winding 0-sequence voltage
v_{dc}	Control winding d-sequence voltage
v_{qc}	Control winding q-sequence voltage
v_{0p}	Power winding 0-sequence voltage
v_{dp}	Power winding d-sequence voltage
v_{qp}	Power winding q-sequence voltage

v_{drcx} Rotor loop x d-sequence voltage from coupling to the control winding (= 0)

v_{qrcx} Rotor loop x q-sequence voltage from coupling to the control winding (= 0)

v_{drpx} Rotor loop x d-sequence voltage from coupling to the power winding (= 0)

v_{qrpx} Rotor loop x q-sequence voltage from coupling to the power winding (= 0)

Use of Multiple Loop Model for Brushless Doubly Fed Machine Rotor Design

Chapter 1
Introduction

The increasing popularity of adjustable speed drives (ASDs) and variable speed generators (VSGs) is driving research to find better solutions than are presently available from induction motors and other conventional machines. While the majority of ASDs use induction machines, this solution has the drawback that the power electronics must process the full kVA rating of the machine. As power converters represent a significant portion of the drive cost, research is focusing on ways to minimize power electronics rating, and, hence, size and cost.

The brushless doubly-fed machine (BDFM) shows promise for converter reduction [1]. Previous work on brushless doubly-fed machines has included work on brushless doubly-fed induction machines and brushless doubly-fed reluctance machines [2]. One variant of the brushless doubly-fed induction machine is the cascaded wound-rotor induction machine, in which two seperate stators excite a wound rotor to achieve variable speed and power factor operation [3]. The BDFM system, shown in Figure 1.1, is an evolutionary step up from the cascaded wound-rotor induction machines in which the wound rotor is replaced with a modified cage rotor, allowing the BDFM to combine the two seperate stators, one for control and one for power windings, into one frame. As with the cascaded wound-rotor induction machine, the special rotor configuration allows for speed control via the control winding. The power winding is fed from the grid and provides the majority of input power to the machine. The control winding is used to adjust the speed of the rotor and power factor of the power winding. The control winding is fed by a converter which, depending on application, can be rated at less than 40% of the machine's rating.

Current distributions in different rotor bars were calculated using three-dimensional finite element analysis, but due to the computationally intensive nature of the analysis, it is impractical to test each design. Rotor bar currents for different designs

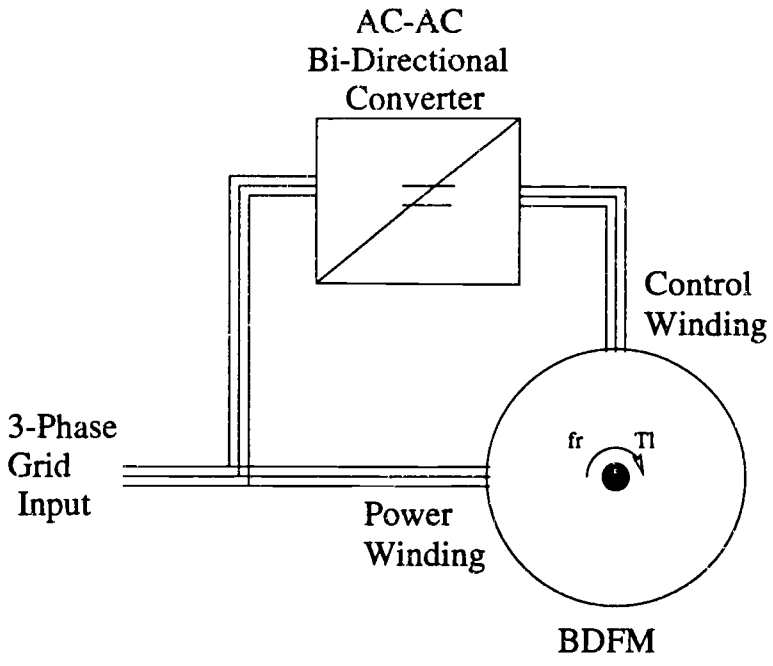

Figure 1.1. BDFM System Diagram

were not known and, in consequence, constructed rotors have used bars of equal area throughout the nests. However, visual observation of heating effects on rotor bars have suggested that their currents are unevenly shared between bars. The outer loops appear to carry the highest currents, while the inner loops carry much lower currents.

This thesis will introduce the BDFM and review some of its important points. Next, the multiple loop model (MLM) for the BDFM and the methods of its use will be described. To confirm the validity of the model, results from the MLM are compared to results from a specially modified BDFM machine and results from finite element simulations. To demonstrate the model's use in design and to develop guidelines for rotor design, a $3.5kW$ general purpose lab machine and a $200kW$, $400Hz$, high-speed, stand-alone aircraft generator are presented.

Chapter 2
Description of BDFM

2.1 General Description

The BDFM has two stator winding systems referred to as the power and control windings. The power winding is fed directly from the grid and the control winding is fed by a converter. The converter needs to be bi-directional, since, depending on the rotor speed and the mode of the machine, the control winding can either generate or absorb energy. A BDFM is generally referred to by the combination of power and control winding pole pairs: a 3 power winding pole pair and 1 control winding pole pair machine is referred to as a "3-1 machine"

Physically, the BDFM is about the size of a comparably rated synchronous machine and, as demonstrated with previously constructed BDFMs, standard National Electrical Manufacturers' Association (NEMA) machine frames can be used. Fitting the BDFM into a NEMA frame is desirable because NEMA frames are widely available and many applications are specified for NEMA frame dimensions.

The speed of the rotor is determined by

$$f_r = \frac{f_p \pm f_c}{P_p + P_c} \tag{2.1}$$

with the sign before f_c denoting positive or negative sequence with respect to the power winding [4] and all frequencies expressed in Hz. According to Equation 2.1, assuming that the power winding is fed with a constant frequency from the grid, the control winding frequency can be used to adjust the rotor frequency.

The "natural speed" of a BDFM is the speed of the rotor with the control winding frequency at 0Hz (dc): for a 3-1 machine with 60Hz on the power winding, the natural speed is $900\frac{r}{min}$. The rating of the control winding is a minimum at the natural speed and rises nearly linearly as the rotor frequency, and therefore the control frequency, deviates from the natural speed.

The "synchronous speed" of a BDFM is the speed at which the rotor mechanical frequency matches the power winding electrical frequency and is determined by

$$f_{synchronous} = \frac{f_p}{P_p} = \frac{f_c}{P_c}. \tag{2.2}$$

Although operating in a mode similar to a synchronous machine, the BDFM relies on induced rotor currents. In consequence, it will not operate at speeds close to the synchronous speed.

Otherwise, the BDFM is operationally similar to a synchronous machine: the BDFM control and synchronous machine field winding are both used to adjust the power factor, but whereas the synchronous machine field winding is excited with dc, the BDFM control winding is excited with ac and can be used to adjust the rotor speed. Further, the BDFM has a load angle, Γ, which can be viewed as similar to a synchronous machine load angle. The synchronous machine load angle determines the torque production and corresponds to the angle of the rotor field with respect to the stator field. The BDFM load angle also determines the torque production of the machine, but corresponds to the angle between the control and power fields after transformation to the *dq*-domain. While the synchronous machine needs brushes to contact the field winding on the rotor, thereby reducing reliability and increasing maintenance, the BDFM has no brushes or contacts and is as robust and reliable as an induction machine.

The primary advantage of the BDFM is that, because of the function of the control winding, across a limited speed range, the converter rating can be held to a fraction of the machine rating. Induction and synchronous machine drive converters are rated for the maximum machine output power derated by efficiency and machine input power factor. For example: a 5hp BDFM for 600-900$\frac{r}{min}$ operation would require a converter rated as low as 1kVA, while an induction motor drive of the same rating would require a converter over 4kVA. Further, in the case of a BDFM operating as a motor, the rectifier side of the converter only carries the real power for the control windings, often less than 20% of the machine rating. Though, depending on circumstance, it could be economical to use the rectifier side of the converter to

boost the power factor from the power winding by supplying reactive VARs to the grid.

2.2 Stator Structure

The stator contains three phase windings for both the control and power windings. Normally, P_p is greater than P_c. On the rotor reference frame, the power and control MMFs have the same frequency, but, due to P_p being greater than P_c, the power winding develops more torque. Since, in the rotor reference frame, the speeds of the power and control winding MMFs are the same, the power winding will have a higher $\omega * Torque$ product and, hence, a higher power output. To avoid transformer coupling of stator windings, P_p and P_c must be different: this difference must be different by more than one pole pair to avoid unbalanced magnetic pull on the rotor. Both windings share the same slots and, generally, integral slot per pole per phase windings are used to avoid the potential for subharmonics. To meet this requirement, the number of stator slots must be factorable by both $3*2*P_p$ and $3*2*P_c$. To reduce spatial harmonic content on the MMF, double-layered fractional pitch windings are used, leading to a complicated stator with four layers per slot and differing slot pitches for the power and control windings.

The stator is very much like that of a pole-changing induction machine. The two main differences are the slot and back iron depths. The slots have to be deeper than conventional induction motors to accomodate the two stator windings. The back iron has to be deeper than a similar speed induction machine in order to accomodate the flux due to the low number of pole-pairs on the control winding in addition to the superimposed power winding flux. With a single pole-pair on the control winding, the concentration of the flux generated by the control winding is very high, so the back iron must be substantial to keep the flux densities to an acceptable level.

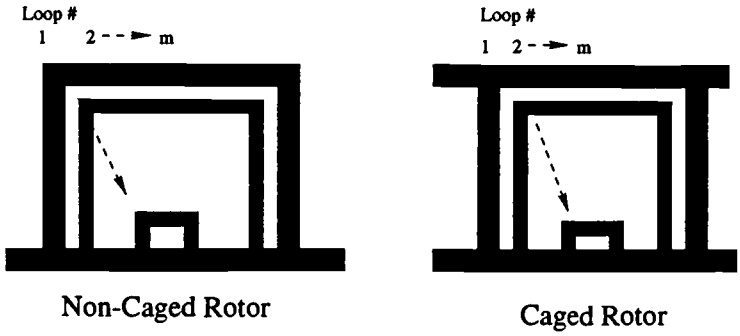

Figure 2.1. BDFM Rotor Structures

2.3 Rotor Structure

The rotor is the enabling feature of the BDFM and is based on work by Creedy [5] and Broadway [6]. BDFM rotors are non-salient and, although previous rotors have used copper bars and endrings, it is anticipated that rotor systems can be die-cast using aluminum. Figure 2.1 shows the two types of rotor structures that can be used: caged and non-caged. A BDFM rotor is composed of P_r "nests", each made up of m loops, and there is a common endring at one end of the rotor. As shown in the figure, the loops are numbered from the outside in. In the caged rotor, an endring joins the outer loop from all nests. In the non-caged rotor, each outer loop, and hence each nest, is isolated from the other and the outer loop is not shared by the adjacent nest.

The number of nests, or rotor poles, is determined by

$$P_r = P_p + P_c, \tag{2.3}$$

so a 3/1 machine would have 4 nests. The number of loops per nest, m, is a tradeoff between harmonic content of the MMF, complexity of construction and allowable flux densities in the rotor steel. The higher m becomes, the lower the harmonic content of the induced MMF, but with the increased copper area, the inter-bar spacing is reduced and inter-bar flux densities increase. Typically, each nest will be composed of 3 to 5 loops.

Previously, all rotor bars have had the same area, but, due to the work on modelling and measuring rotor bar currents, future rotor bars will be scaled to equalize current densities in each rotor bar.

Chapter 3
Multiple Loop Model

3.1 Background

To date, the most extensively used model applied to the analysis of BDFMs has been the steady-state Single Loop Model (SLM). In the first iteration, the SLM was limited to $3-1$ BDFMs [7]. The SLM was then extended to the General Pole Number SLM, which could accomodate any $P_p + P_c$ combination [8]. This model is shown in Fig 3.1. The SLM was based on induction motor theory and looked much like an induction motor model in the rotor reference frame with, as expected, two stator windings. The multiple loops in each rotor nest are aggregated into a single equivalent "loop" circuit in the model in a manner similar to induction motor models. In the derivation of the model, the currents in the corresponding loops of each nest were assumed to be equal, although it was acknowledged that there could be differences in magnitudes between the loops within the nests themselves.

The SLM was programmed in Matlab, as Matlab combines matrix functions and easily modifiable, portable scripts with full graphing capabilities and a powerful command line. In one or two instances, the model was implemented in C [9] [10], but these programs were difficult to keep current or to transition between successive graduate researchers and were used little after the Matlab version was developed.

During maintenance of an experimental laboratory BDFM, discoloration of each nest's outer loops was observed. This indicated that the outer loops of the nests had been subject to much higher temperatures during operation than the inner loops. This observation strongly suggested that currents in the outer loops were much higher than in the inner loops. The first effort to investigate this problem was conducted using a finite element analysis simulation [11]. After the finite element analysis confirmed that rotor loop currents were unevenly shared by the rotor bars, the SLM

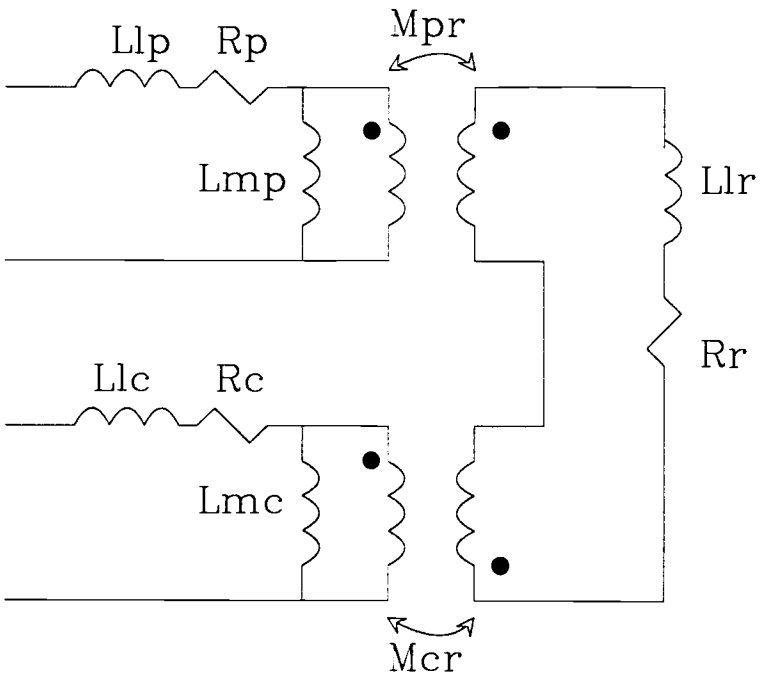

Figure 3.1. Single Loop Model Circuit

was modified to model each rotor bar as a separate rotor circuit. This thesis is the first presentation of that Multiple Loop Model.

3.2 Development of the Model

The theoretical extension of the SLM to the Multiple Loop Model(MLM) was done by Michael S. Boger[12]. Programming of the low level MLM routines was also done by Michael Boger.

The model is graphically depicted in Figure 3.2. As depicted in the figure and as presently programmed, the model assumes that the rotor bars are equally spaced and that the section of endring joining them are of equal length.

Whereas the Single Loop Model aggregated the rotor loops into a single equivalent loop, the Multiple Loop Model depicts each rotor loop as a seperate circuit in the model. Since the rotor is symmetrical around each nest, the model only represents

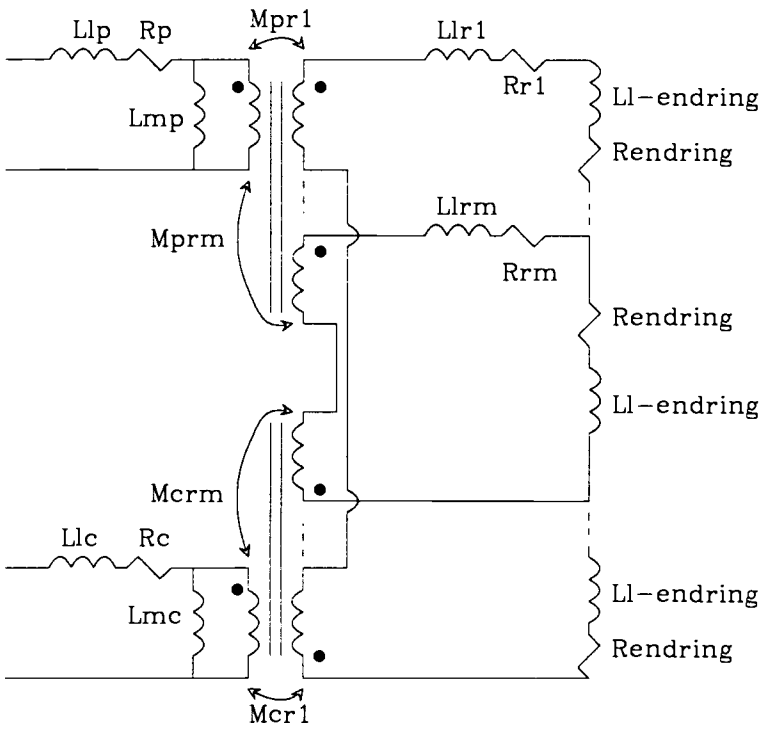

Figure 3.2. Multiple Loop Model Circuit

one nest and assumes that there will be $P_p + P_c$ nests in the rotor.

3.2.1 Dynamic Model

For the dynamic model of the BDFM, the complete voltage equation, as developed by Boger, for the MLM is

$$\mathbf{v} = (\mathbf{R} + \frac{\mathbf{d}}{\mathbf{dt}}\mathbf{L} + \omega_r\overline{\mathbf{L}})\mathbf{i}, \tag{3.4}$$

where:

$$\mathbf{R} = \begin{bmatrix}
r_p & 0 & 0 & 0 & 0 & 0 & 0 & 0 & 0 & 0 & \cdots & 0 & 0 & 0 & 0 \\
0 & r_p & 0 & 0 & 0 & 0 & 0 & 0 & 0 & 0 & \cdots & 0 & 0 & 0 & 0 \\
0 & 0 & r_p & 0 & 0 & 0 & 0 & 0 & 0 & 0 & \cdots & 0 & 0 & 0 & 0 \\
\hline
0 & 0 & 0 & r_c & 0 & 0 & 0 & 0 & 0 & 0 & \cdots & 0 & 0 & 0 & 0 \\
0 & 0 & 0 & 0 & r_c & 0 & 0 & 0 & 0 & 0 & \cdots & 0 & 0 & 0 & 0 \\
0 & 0 & 0 & 0 & 0 & r_c & 0 & 0 & 0 & 0 & \cdots & 0 & 0 & 0 & 0 \\
\hline
0 & 0 & 0 & 0 & 0 & 0 & r_{r11} & 0 & 0 & 0 & \cdots & r_{rm1} & 0 & 0 & 0 \\
0 & 0 & 0 & 0 & 0 & 0 & 0 & r_{r11} & 0 & 0 & \cdots & 0 & r_{rm1} & 0 & 0 \\
\hline
0 & 0 & 0 & 0 & 0 & 0 & 0 & 0 & r_{r11} & 0 & \cdots & 0 & 0 & r_{rm1} & 0 \\
0 & 0 & 0 & 0 & 0 & 0 & 0 & 0 & 0 & r_{r11} & \cdots & 0 & 0 & 0 & r_{rm1} \\
\hline
 & \vdots & & & \vdots & & \vdots & \vdots & \vdots & \vdots & \ddots & \vdots & \vdots & \vdots & \vdots \\
\hline
0 & 0 & 0 & 0 & 0 & 0 & r_{r1m} & 0 & 0 & 0 & \cdots & r_{rmm} & 0 & 0 & 0 \\
0 & 0 & 0 & 0 & 0 & 0 & 0 & r_{r1m} & 0 & 0 & \cdots & 0 & r_{rmm} & 0 & 0 \\
\hline
0 & 0 & 0 & 0 & 0 & 0 & 0 & 0 & r_{r1m} & 0 & \cdots & 0 & 0 & r_{rmm} & 0 \\
0 & 0 & 0 & 0 & 0 & 0 & 0 & 0 & 0 & r_{r1m} & \cdots & 0 & 0 & 0 & r_{rmm}
\end{bmatrix} \tag{3.5}$$

$$\mathbf{L} = \begin{bmatrix}
L_p & 0 & 0 & 0 & 0 & 0 & M_{pr1} & 0 & M_{pr1} & 0 & \cdots & M_{prm} & 0 & M_{prm} & 0 \\
0 & L_p & 0 & 0 & 0 & 0 & 0 & M_{pr1} & 0 & -M_{pr1} & \cdots & 0 & M_{prm} & 0 & -M_{prm} \\
0 & 0 & L_p & 0 & 0 & 0 & 0 & 0 & 0 & 0 & \cdots & 0 & 0 & 0 & 0 \\
\hline
0 & 0 & 0 & L_c & 0 & 0 & M_{cr1} & 0 & M_{cr1} & 0 & \cdots & M_{crm} & 0 & M_{crm} & 0 \\
0 & 0 & 0 & 0 & L_c & 0 & 0 & -M_{cr1} & 0 & M_{cr1} & \cdots & 0 & -M_{crm} & 0 & M_{crm} \\
0 & 0 & 0 & 0 & 0 & L_c & 0 & 0 & 0 & 0 & \cdots & 0 & 0 & 0 & 0 \\
\hline
M_{pr1} & 0 & 0 & 0 & 0 & 0 & L_{lr1} & 0 & 0 & 0 & \cdots & L_{lrm1} & 0 & 0 & 0 \\
0 & M_{pr1} & 0 & 0 & 0 & 0 & 0 & L_{lr1} & 0 & 0 & \cdots & 0 & L_{lrm1} & 0 & 0 \\
\hline
0 & 0 & 0 & M_{cr1} & 0 & 0 & 0 & 0 & L_{lr1} & 0 & \cdots & 0 & 0 & L_{lrm1} & 0 \\
0 & 0 & 0 & 0 & M_{cr1} & 0 & 0 & 0 & 0 & L_{lr1} & \cdots & 0 & 0 & 0 & L_{lrm1} \\
\hline
 & \vdots & & & \vdots & & \vdots & \vdots & \vdots & \vdots & \ddots & \vdots & \vdots & \vdots & \vdots \\
\hline
M_{prm} & 0 & 0 & 0 & 0 & 0 & L_{lr1m} & 0 & 0 & 0 & \cdots & L_{lrmm} & 0 & 0 & 0 \\
0 & M_{prm} & 0 & 0 & 0 & 0 & 0 & L_{lr1m} & 0 & 0 & \cdots & 0 & L_{lrmm} & 0 & 0 \\
\hline
0 & 0 & 0 & M_{crm} & 0 & 0 & 0 & 0 & L_{lr1m} & 0 & \cdots & 0 & 0 & L_{lrmm} & 0 \\
0 & 0 & 0 & 0 & M_{crm} & 0 & 0 & 0 & 0 & L_{lr1m} & \cdots & 0 & 0 & 0 & L_{lrmm}
\end{bmatrix} \tag{3.6}$$

$$\overline{\mathbf{L}} = \left[\begin{array}{ccc|ccc|cc|cc|c|cc|cc} 0 & P_pL_p & 0 & 0 & 0 & 0 & P_pM_{pr1} & 0 & -P_pM_{pr1} & \cdots & 0 & P_pM_{prm} & 0 & -P_pM_{prm} \\ -P_pL_p & 0 & 0 & 0 & 0 & 0 & 0 & -P_pM_{pr1} & 0 & \cdots & -P_pM_{prm} & 0 & -P_pM_{prm} & 0 \\ 0 & 0 & 0 & 0 & 0 & 0 & 0 & 0 & 0 & \cdots & 0 & 0 & 0 & 0 \\ \hline 0 & 0 & 0 & 0 & P_cL_c & 0 & -P_cM_{cr1} & 0 & P_cM_{cr1} & \cdots & 0 & -P_cM_{crm} & 0 & P_cM_{crm} \\ 0 & 0 & 0 & -P_cL_c & 0 & 0 & 0 & -P_cM_{cr1} & 0 & \cdots & -P_cM_{crm} & 0 & -P_cM_{crm} & 0 \\ 0 & 0 & 0 & 0 & 0 & 0 & 0 & 0 & 0 & \cdots & 0 & 0 & 0 & 0 \\ \hline 0 & 0 & 0 & 0 & 0 & 0 & 0 & 0 & 0 & \cdots & 0 & 0 & 0 & 0 \\ 0 & 0 & 0 & 0 & 0 & 0 & 0 & 0 & 0 & \cdots & 0 & 0 & 0 & 0 \\ \hline 0 & 0 & 0 & 0 & 0 & 0 & 0 & 0 & 0 & \cdots & 0 & 0 & 0 & 0 \\ 0 & 0 & 0 & 0 & 0 & 0 & 0 & 0 & 0 & \cdots & 0 & 0 & 0 & 0 \\ \hline \vdots & & & \vdots & & & \vdots & \vdots & \vdots & \ddots & \vdots & \vdots & \vdots & \vdots \\ \hline 0 & 0 & 0 & 0 & 0 & 0 & 0 & 0 & 0 & \cdots & 0 & 0 & 0 & 0 \\ 0 & 0 & 0 & 0 & 0 & 0 & 0 & 0 & 0 & \cdots & 0 & 0 & 0 & 0 \\ \hline 0 & 0 & 0 & 0 & 0 & 0 & 0 & 0 & 0 & \cdots & 0 & 0 & 0 & 0 \\ 0 & 0 & 0 & 0 & 0 & 0 & 0 & 0 & 0 & \cdots & 0 & 0 & 0 & 0 \end{array}\right] \tag{3.7}$$

$$\mathbf{v} = \left[\begin{array}{c} v_{qp} \\ v_{dp} \\ v_{0p} \\ \hline v_{qc} \\ v_{dc} \\ v_{oc} \\ \hline v_{qrp1} = 0 \\ v_{drp1} = 0 \\ \hline v_{qrc1} = 0 \\ v_{qrc1} = 0 \\ \hline \vdots \\ \hline v_{qrpm} = 0 \\ v_{drpm} = 0 \\ \hline v_{qrcm} = 0 \\ v_{qrcm} = 0 \end{array}\right] \tag{3.8}$$

$$\mathbf{i} = \left[\begin{array}{c} i_{qp} \\ i_{dp} \\ i_{0p} \\ \hline i_{qc} \\ i_{dc} \\ i_{oc} \\ \hline i_{qrp1} \\ i_{drp1} \\ \hline i_{qrc1} \\ i_{qrc1} \\ \hline \vdots \\ \hline i_{qrpm} \\ i_{drpm} \\ \hline i_{qrcm} \\ i_{qrcm} \end{array}\right] \tag{3.9}$$

The instantaneous torque produced by the motor is given by

$$T_e = P_p \sum_{j=1}^{m} \mathbf{M}_{pj}(i_{qp}i_{drj} - i_{dp}i_{qrj}) - P_c \sum_{j=1}^{m} \mathbf{M}_{cj}(i_{qc}i_{drj} + i_{dc}i_{qrj}). \tag{3.10}$$

In equation 3.8, the rotor loop voltages are equated to 0, because the rotor loops are isolated circuits and, as such, there can be no forcing voltage on the rotor.

Equations 3.5 & 3.6 show that each loop voltage equation is not a simple function of a single loop, as was assumed in the Single Loop Model. Following the loop current around the loop, a loop's voltage drop due to resistance is

$$v_{qrp1-resistive} = i_{qrp1}r_{r11} + i_{qrp2}r_{r21} + ... + i_{qrpm}r_{rm1}. \tag{3.11}$$

r_{r11} represents the resistance of the isolated portion of the loop, so the voltage drop would be $i_{qrp1}r_{r11}$. All loop currents are summed in the innermost portion of the common endring and, consequently, each loop current causes a mutual voltage drop in the section which it shares with the outer loops. By superposition, the resistive voltage drop around loop 1 has a component due to the current in loops $2 \rightarrow m$ passing through the small section of the common endring joining the ends of the isolated portion of loop 1.

As shown in Equation 3.6, the common leakage inductances of the endring have a similar effect as the common resistances of the endring: the leakage inductances cause the loop voltage equation of each loop to be dependent on the currents in all other loops. These effects are in addition to the mutual, active fluxes of the rotor loops.

For completeness, the zero sequence components are included in this model. In steady-state modelling, the motor and its supplies are assumed to be balanced, so that the zero sequence components can be ignored.

3.2.2 Steady-State Model

The steady-state MLM model for the BDFM is given in Equation 3.12. The steady state torque for the MLM is given in Equations 3.13, 3.14 and 3.15. The steady-state MLM model was derived using the same procedures as the simplification of the general-pole number SLM dynamic model to the steady state model [13]. While the dynamic model of the BDFM is useful for determining transient response and reaction to imbalances, the simulation time is very long. The steady-state model,

compared to the dynamic model, is relatively simple and runs very quickly. For motor design and investigation of motor performance, the steady-state model is adequate and appropriate.

"$\mp$" in Equation 3.12 refers to the sequence of the control winding with respect to the power winding. If the control winding sequence is positive with respect to the power winding, then the sign is negative.

Γ is the electrical angle between the power and control winding excitations, $\angle(V_q p - V_q c)$. Γ is a parameter of the MLM programs and is often used in discussion of BDFM motor design.

$$\left[\begin{array}{c} V_{qp} \\ V_{qc} \\ \hline V_{qr1} \\ \vdots \\ V_{qrm} \end{array}\right] = \left[\begin{array}{cc|ccc} r_p + j\omega_p L_{lp} & 0 & j\omega_p M_{pr1} & \cdots & j\omega_p M_{prm} \\ 0 & r_c \mp j\omega_c L_{lc} & \mp j\omega_c M_{cr1} & \cdots & \mp j\omega_c M_{crm} \\ \hline j\omega_R M_{pr1} & j\omega_R M_{cr1} & r_{r11} + j\omega_R Lr11 & \cdots & r_{r1m} + j\omega_R Lr1m \\ \vdots & \vdots & \vdots & \ddots & \cdots \\ j\omega_R M_{prm} & j\omega_R M_{crm} & r_{rm1} + j\omega_R Lrm1 & \cdots & r_{rmm} + j\omega_R Lrmm \end{array}\right] \left[\begin{array}{c} I_{qp} \\ I_{qc} \\ \hline I_{qr1} \\ \vdots \\ I_{qrm} \end{array}\right] \tag{3.12}$$

$$T_{ep} = 3P_p \sum_{i=1}^{m} (M_{pi}[\Im(I_{qp})\Re(I_{qr}) - \Re(I_{qp})\Im(I_{qr})]) \tag{3.13}$$

$$T_{ec} = -3P_c \sum_{i=1}^{m} (M_{ci}[\Im(I_{qc})\Re(I_{qr}) - \Re(I_{qp})\Im(I_{qr})]) \tag{3.14}$$

$$T_e = T_{ep} + T_{ec} \tag{3.15}$$

3.3 Sample Model Parameters

Equations 3.16, 3.17, 3.18 and 3.19 show mutual inductance between the power winding and the rotor, mutual inductance between the control winding and the rotor, the rotor resistance matrix and the rotor inductance matrix. The values are for a 5hp BDFM, discussed in Chapter 5, designed for demonstration purposes.

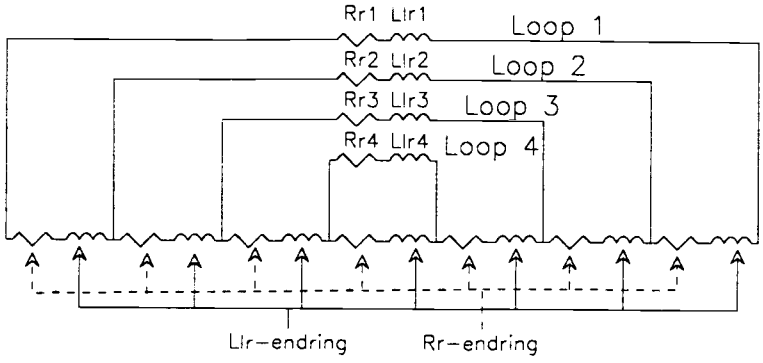

Figure 3.3. Diagram of Rotor Nest with 4 Loops

$$M_{pr} = \begin{bmatrix} 0.394mH \\ 0.553mH \\ 0.471mH \\ 0.184mH \end{bmatrix} \tag{3.16}$$

$$M_{cr} = \begin{bmatrix} 1.84mH \\ 1.38mH \\ 0.86mH \\ 0.29mH \end{bmatrix} \tag{3.17}$$

$$R_r = \begin{bmatrix} 9.74e-05 & 2.97e-06 & 1.78e-06 & 5.94e-07 \\ 2.97e-06 & 2.18e-05 & 1.78e-06 & 5.94e-07 \\ 1.78e-06 & 1.78e-06 & 2.57e-05 & 5.94e-07 \\ 5.94e-07 & 5.94e-07 & 5.94e-07 & 2.76e-05 \end{bmatrix} \Omega \tag{3.18}$$

$$L_r = \begin{bmatrix} 2.75e-05 & 1.89e-05 & 1.13e-05 & 3.79e-06 \\ 1.89e-05 & 1.90e-05 & 1.13e-05 & 3.79e-06 \\ 1.13e-05 & 1.13e-05 & 1.15e-05 & 3.79e-06 \\ 3.79e-06 & 3.79e-06 & 3.79e-06 & 3.99e-06 \end{bmatrix} H \tag{3.19}$$

As discussed in Section 3.2.1, the R_r and L_r matrices describe how the loop currents interact with other loops voltages. This relationship is pictured in Figure 3.3. For example, the voltage around loop 1 not only includes the voltage drop due to the current in loop 1, but includes the voltage drop due to loop current 2 as it passes through 5 lengths of the common endring, the voltage drop due to loop current 3 as it passes through 3 lengths of the common endring and the voltage drop due to loop current 4 as it passes through 1 length of the common endring. One length of the common endring is the distance along the endring between sucessive loop connections. In Equation 3.18, each length has a resistance of $.594u\Omega$ and in Equation 3.19, each length has an inductance of $3.79uH$.

3.4 Model Implentation

The steady state Multiple Loop Model has been implemented as a hierarchy of functions in Matlab. Matlab scripts discussed below or relevant to this thesis are given in [14]. While many programs have been developed to use the MLM, the MLM essentially consists of two computational "kernels",*mlcapability* and *mlsolve*, each of which is composed of a core of fuctions. The hierarchy is depicted in Figure 3.4.

The core modules of the Multiple Loop Model are :

mlmodel : This file is generated by one of the design programs and contains the parameters for the model of the machine being simulated. It is typically read in by any procedure needing to know the machine parameters.

mlsetup : This file sets up the excitation parameters, such as control and power winding frequency, control and power winding excitation magnitude, and rotor electrical and mechanical frequency.

mlz : This file returns the impedance matrix for the multiple loop model, given rotor, and control and power winding electrical frequencies.

mltorque : This file returns the steady state torque for the motor, given Γ and stator currents.

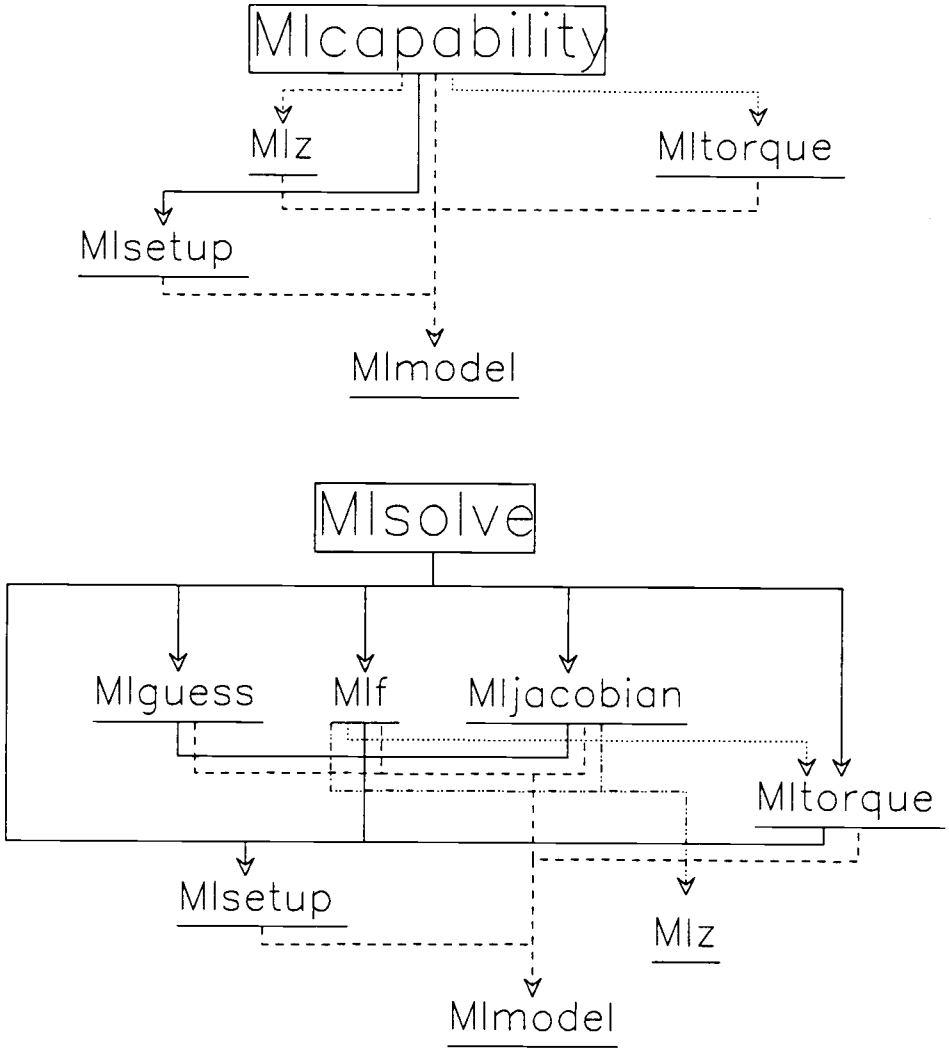

Figure 3.4. MLM Program Hierarchy

mljacobian : This file calculates the Jacobian matrix given the states, control voltage and shaft speed.

mlf: This file evaluates the Newton-Raphson functions given the states, control voltage, load torque and shaft speed.

mlguess : This file calculates the initial states of the system given control voltage, Γ and shaft speed.

The first of the kernels (*mlcapability*) calculates the set of torques produced by the motor given a set of current inputs for the power and control windings, a set of load angles, Γs, and power and control excitation frequencies. This routine is often used to quickly calculate motor performance by setting stator excitation values and sweeping through a coarse range of Γ. Typically, a program utilizing this kernel will need to calculate 10-30 different control voltage excitation sweeps. Each sweep will consist of 20-100 seperate Γ points, necessitating a quick procedure. In this case, Γ is a function parameter and load torque is a calculated quantity.

The second of the kernels (*mlsolve*) implements a Newton-Raphson solution to the steady-state equations. The Newton-Raphson solution takes, as input, the power and control voltages, power and control excitation frequencies, and the target load torque and predicts the motor performance. Whereas the first kernel used a set of Γ values to calculate a set of motor torques, the Newton-Raphson method is used when stator voltages and load torque are known and an accurate prediction of motor performance is to be calculated. In this case, load torque is a function parameter and Γ is a calculated quantity.

The MLM would typically be used as follows:

- For a range of Γ, *mlcapability* would be used to solve for the currents for the power and control windings, based on rotor speed and stator excitation values.
- The above step would be repeated for different values of control winding excitation until the desired operating point, such as a certain load torque and power winding power factor, were found.

- If a more accurate prediction of motor performance were required, using the power and control winding voltage, the speed of the rotor and the target load torque, *mlsolve* would be used to calculate the machine performance.
- For each speed, torque or power winding power factor point, the above steps would be repeated.

3.5 Design Programs

Two programs used to design BDFM systems using the MLM are *mlspeedmot* and *mlspeedgen*. *mlspeedmot*, as the name suggests, is designed to calculate motor performance across a speed range. *mlspeedgen* works very much as *mlspeedmot* does, except that *mlspeedgen* predicts stand alone generator performance.

During the development of these programs, a number of difficulties with BDFM simulation were found. These are discussed in Appendix A.

3.5.1 *mlspeedmot*

mlspeedmot is used to predict performance of a BDFM operating as a motor with power winding power factor, rotor speed and load torque specified by the user. *mlspeedmot* is designed to simulate a range of speeds, torques and power factors in one run, usually in less than 4-5 minutes. Before *mlspeedmot*, simulations took 15 minutes and the target power factor was set to unity.

mlspeedmot works as follows:

(1) Given shaft speed, desired output torque and power winding power factor, guess at a control voltage and do:

   (a) Calculate motor currents and torques using *mlcapability* and the control voltage.

   (b) Calculate power winding power factor using results from (a).

(c) If torque output and power factor are satisfactory, then return with results.

(d) If torque output is satisfactory, but power factor is low, then increase control voltage and return to (a).

(e) If torque output is satisfactory, but power factor is high, then decrease control voltage and return to (a).

(f) If torque output is high, then decrease control voltage and return to (a).

(g) If torque output is low, then increase control voltage and return to (a).

(2) Write results to data file.

(3) If there are more combinations of shaft speed, torque output and power winding power factor to be simulated, return to (1).

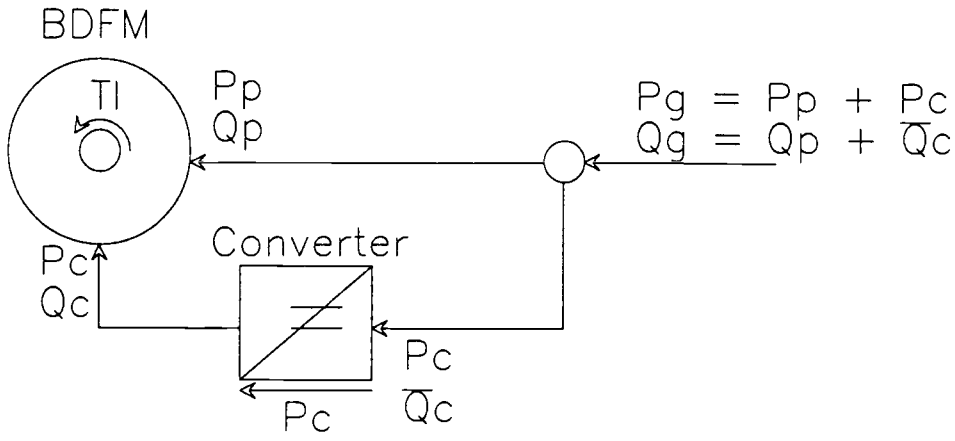

Figure 3.5. Power Flow for BDFM Generator

3.5.2 *mlspeedgen*

mlspeedgen is based on *mlspeedmot*, and their inputs and outputs are identical, *mlspeedgen* typically takes 10 minutes to run.

mlspeedgen is used to predict BDFM performance when operating as a stand-alone generator system across a user defined range of output power factor, rotor speed and system power output. As shown in Figure 3.5, in a stand alone generator system, the inputs of the power and control windings are summed at the grid, making for a complicated simulator due to fixed grid power requirements and the varying sum of power and control inputs.

On the side of the control converter connected to the control windings, only real power, P_c, is transferred across the dc-link to the windings and the reactive power, Q_c, is circulated between the control windings and the converter. The side of the control converter connected to the grid takes in the real power for the control windings and, if a voltage source converter input is assumed, the reactive power, $\bar{Q}_c$, is determined by the load impedance and the power winding reactive power output, Q_p. For a "worst case" generator system, the load could have a 0.7 lagging power factor and a typical P_c would be around 25% of the machine rating, giving a rating for the rectifier side of the converter at 35% of the machine rating.

mlspeedgen works as follows:

(1) Given shaft speed, desired system output power and system power factor, guess at a control voltage and do:

   (a) Calculate motor currents using *mlcapability* and the control voltage.

   (b) Calculate power flow and power factor in system using results from (a).

   (c) If power flow and power factor are satisfactory, then return with results.

   (d) If power flow is satisfactory, but power factor is low then increase control voltage and return to (a).

   (e) If power flow is satisfactory, but power factor is high then decrease control voltage and return to (a).

   (f) If power flow is high, then decrease control voltage and return to (a).

   (g) If power flow is low, then increase control voltage and return to (a).

(2) Write results to data file.

(3) If there are more combinations of shaft speed, system power output and system power factor to be simulated, return to (1).

Chapter 4
Verification of the Model

After the model had been developed and before it could be relied upon for design use, verification was needed. This was accomplished by comparing it to two other methods of determining rotor currents.

4.1 Finite Element Analysis

Investigation of rotor current distribution was first carried out using a finite element analysis of the BDFM [11]. While finite element analysis is difficult and time-consuming in its own right, analysis of the BDFM is further complicated by the structure of the motor:

- the nested-loop rotor construction, having isolated conductors on one end and a common end-ring on the other, requires a 3-dimensional model;
- there are two seperate sources of stator excitation;
- except at standstill, the power winding, the control winding and the rotor all operate at different frequencies and with a combination of sequences;
- the complete machine, with P_p and P_c pole-pairs on the stator and P_r poles on the rotor, has no obvious periodic boundaries, which would enable the analysis to be based on a small section of the machine;
- no *a priori* knowledge of the rotor current was assumed, so the eddy-current approach to finite element modelling had to be used.

4.1.1 Simplification of the Finite Element Analysis

An unsimplified, 3-dimensional, 360° finite element analysis of the BDFM would require over 8000 grid points. To make the finite element analysis easier to implement, the machine description was simplified as much as possible:

- viewed from the rotor electrical reference frame, the two seperate stator-induced MMFs in the airgap appear as two MMFs rotating at equal but opposite frequencies. Placing these conditions on the finite element model results in an alternating periodic boundary over the lesser of either P_p or P_c.
- except for the ends of the rotor, the rotor has axial symmetry. A coarse mesh can be used to represent the rotor bars and steel. For the isolated endrings and the common endring, a fine mesh must be used to describe the detail.

Using these simplifications, the number of grid points used for a highly detailed simulation of the BDFM was about 50% of the unsimplified model.

4.1.2 Comparison to the Multiple Loop Model

Specifications for the motor simulated in the Finite Element Analysis and by the MLM are shown in Table 1. The power winding was excited using 60Hz and the control winding was excited using 20Hz [11]. The excitation magnitudes used in the two simulations were different, so results have been normalized for comparison.

Figure 4.1 shows a comparison between the predictions of the Finite Element Analysis and the Multiple Loop Model. The results of the Finite Element Analysis suggest that the MLM duplicates, within a reasonable error due to modelling differences, the predictions of the FEA.

4.2 Experimental Verification

In order to obtain test data for BDFM rotor current distribution, a laboratory BDFM was modified to enable rotor loop currents to be measured directly. The test ma-

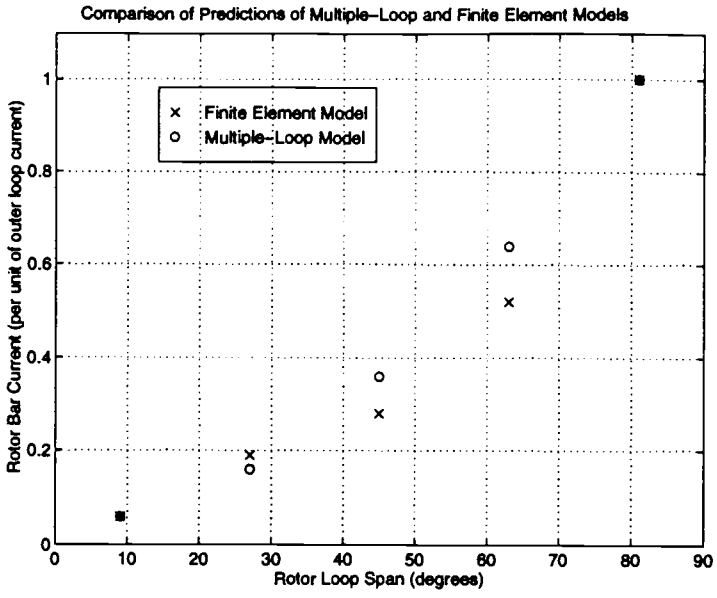

Figure 4.1. Comparison of Finite Element Analysis and Multiple Loop Model

chine's rotor had the usual solid bar endring and nest structure removed. The rotor was then re-wound using flexible, insulated 16 AWG wire. At one end of the rotor, the wire was stripped and a commong endring was soldered together. One nest was threaded with loops long enough to be pulled out through the frame vents. The individual loop currents were then measurable using a *Fluke 41 Power Harmonics Analyzer.*

Due to the wire loops being drawn out through the frame vents and preventing rotor movement, this setup was only useful for standstill measurements. In order to guarantee that the rotor did not move during testing, the rotor was blocked.

Using long loops in one nest caused the rotor to be asymmetrical and invalidated a major assumption of the Multiple Loop Model. Depending on the loop number, the long loops probably had $50\% - 75\%$ more resistance than other nests' loops. The MLM model of the machine used rotor loop resistances which were adjusted to be about 15% higher than the regular wire loops in the machine. The inductance of the long loop was not much larger than the normal loops due to the low μ_r of air

5hp Machine Description			
Slots	36	Slot Pitch	10°
Slot+Tooth Width	1.31cm	Slot Depth	2cm
$\frac{Slots}{pole*phase}$		Winding Pitch	
Power Winding	2	Power Winding	150°
Control Winding	6	Control Winding	120°
$\frac{Turns}{Coil}$		Back Iron Depth	2cm
Power Winding	8		
Control Winding	8		

Table 1. Experimental Machine Description

compared to the μ_r of steel.

Details of the experimental machine are presented in Table 1.

4.2.1 Experimental Procedure

According to equation 2.1, for the rotor to be at standstill, the control winding frequency has to be the opposite of the power winding frequency. To meet this requirement, the control and power windings were excited from the same source, but the control winding had two phases interchanged, thereby reversing the sequence.

A 3ϕ, $60Hz$, $230V_{ll}$ input auto-transformer was used to excite the two windings. The output voltage was increased until a reasonable current ($\approx 10A$ for 16 AWG wire) was obtained in the rotor common endring.

To test different load angles (Γ), a *Mitutoy 360 Digital Protractor* was attached to the rotor bar. The rotor was rotated until the sum of the rotor bar currents was minimized, at which point the digital protractor was set to 0°. Loop current measurements were taken and the rotor angle was increased in increments of 22.5°, until the sum of loop currents was maximum at 90°.

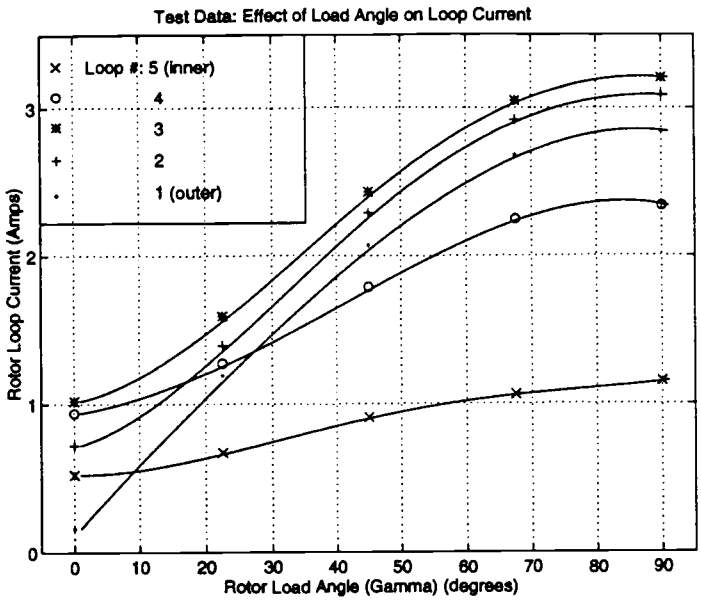

Figure 4.2. Experimental Measurements of Rotor Loop Currents

Measurements of rotor loop currents taken from the modified machine are shown in Figure 4.2.

4.2.2 Comparison to the Multiple Loop Model

The Multiple Loop Model was provided with the experimental machine's parameters, power and control winding excitation, and rotor speed. With the given operating conditions, the BDFM will produce minute amounts of torque. Because the program which solves the BDFM equations solves for a target torque and not for Γ , the load torque was adjusted until the returned Γ was equal to each Γ taken using the experimental setup.

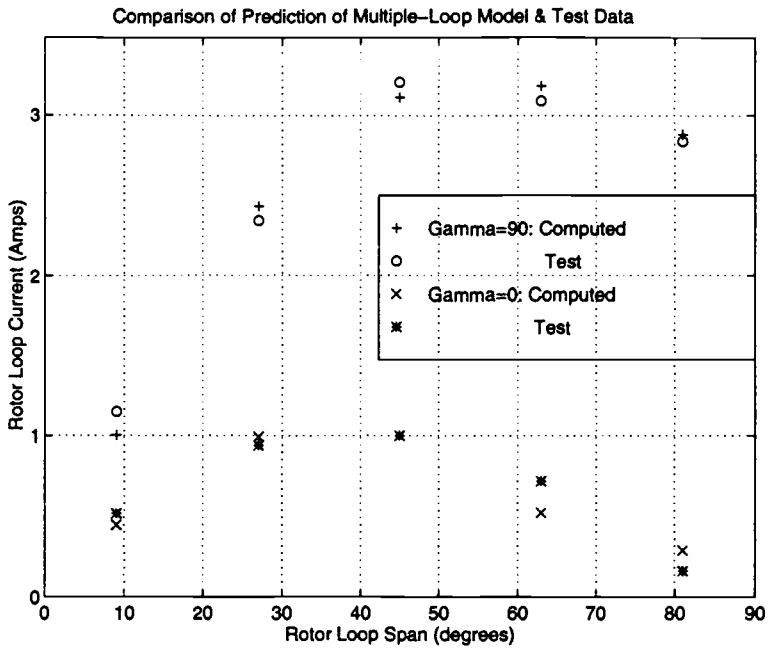

Figure 4.3. Comparison of Test Results with Multiple Loop Model

The results of the MLM's predictions are compared to the experimental results in Figure 4.3. The MLM results agreed very closely with the experimental data, often to within 10%, suggesting that the MLM accurately represents the rotor current operation and values.

Chapter 5
$5Hp$ Demonstration Drive

The first project is the development of a 5hp drive to be used to demonstrate the BDFM to prospective producers and customers. This is a "pre-production" drive designed to be easily portable, to operate over a wide speed range and to operate as either a generator or as a motor. Concurrent to the design of the motor, a bi-directional, 3-phase, unity input power factor, 2kVA converter is being designed and constructed by other members of the BDFM research group. The system is not optimally designed for any one practical application, as it sacrifices maximum efficiency to get maximum flexibility. One objective is for the system to fit in the back of a pick-up truck or in a large car trunk, so that it can be carried to demonstration sites.

The design goals for this motor are:

- Operate over a wide speed range. Be able to demonstrate the motor operating over $100 \rightarrow 1100\frac{r}{min}$ with no load torque applied.
- Operate the system over $600 \rightarrow 900\frac{r}{min}$ with the applied torque following the cubic power curve. At $900\frac{r}{min}$, the motor will be able to put out 3.5kW.
- Operate the system as a generator over $1300 \rightarrow 1800\frac{r}{min}$. Demonstrate that the BDFM will generate well at high speed.
- Operate the system over $600 \rightarrow 900\frac{r}{min}$ with a constant load torque.
- Fit the motor into a NEMA induction motor frame. NEMA induction motor frames are readily available, so cost will be kept to a minimum.
- Try to fit the motor into as close a frame size as would hold an induction machine of similar rating.

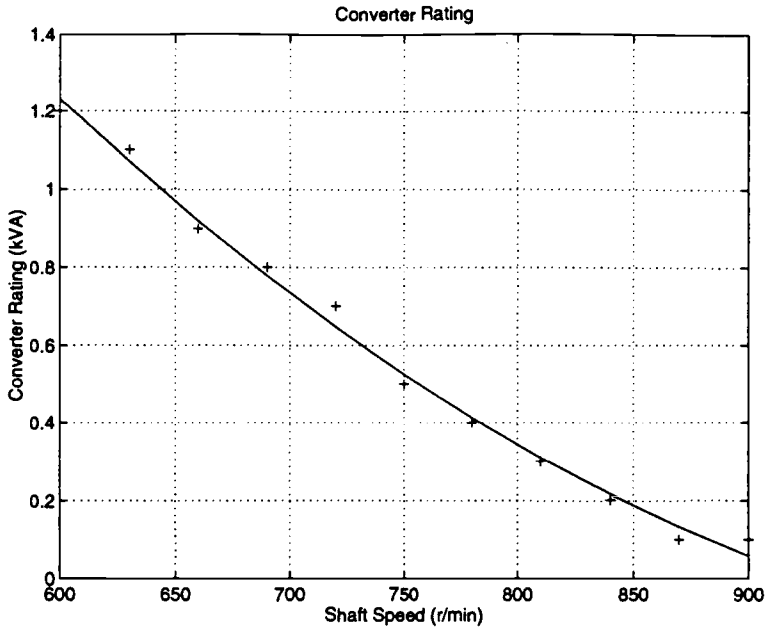

Figure 5.1. Square Pole Machine : Converter Rating : Pump Load

5.1 The Two Design Approaches

The design of the motor was approached in two different ways: by sizing the motor to get "square-poles"on the rotor and by sizing the motor to fit the smallest NEMA frame possible as limited by saturation. Table 2 provides a comparison between the dimensions of the two designs. Figures 5.1, 5.2, 5.3 and 5.4 show selected converter ratings and efficiencies of the two designs.

The "square pole" approach was tried first. Poles are rectangular and, since a square provides the most area per circumference, a square pole produces the maximum flux, which is proportional to area, for the least conductor. As shown in Table 2, the square pole design approach produced a "pancake" machine, very flat ($11cm(4.3")$) and very wide ($38cm(15")$). Due to the diameter of the machine, this approach requires a $324T$ NEMA frame, which would otherwise house a $20hp$, $900\frac{r}{min}$ induction machine.

In the second design, the rotor diameter was reduced to $15cm$ (6.5") and the rotor length was increased to $15cm$ (6.5"). The "NEMA-frame" machine requires a

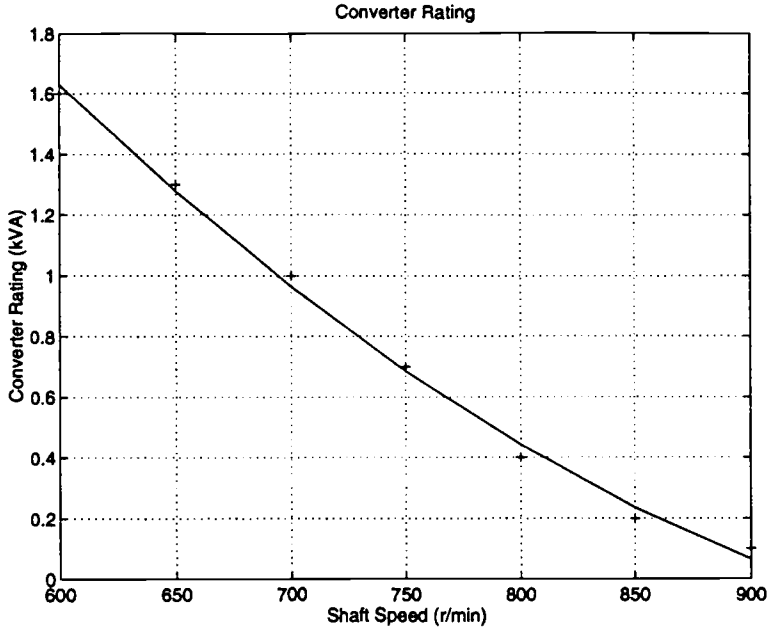

Figure 5.2. "NEMA" Design : Converter Rating : Pump Load

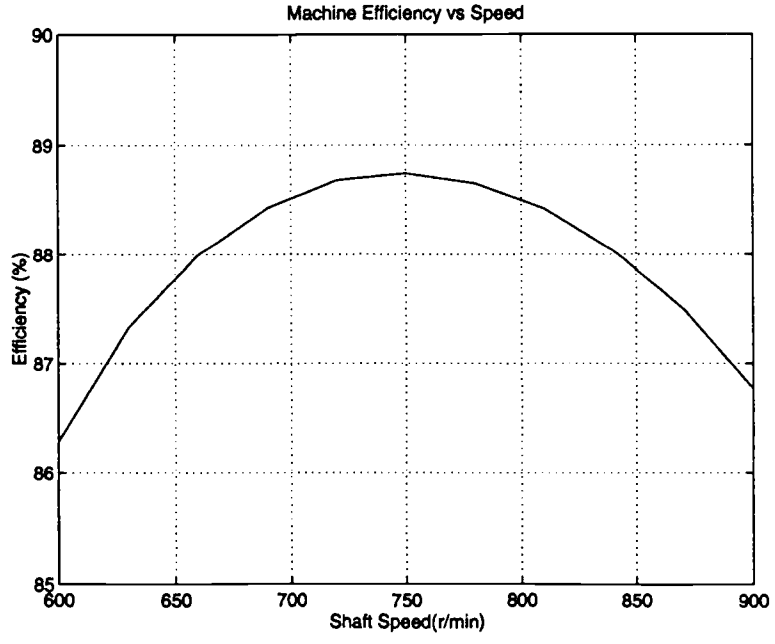

Figure 5.3. Square Pole Design : Machine Efficiency : Pump Load

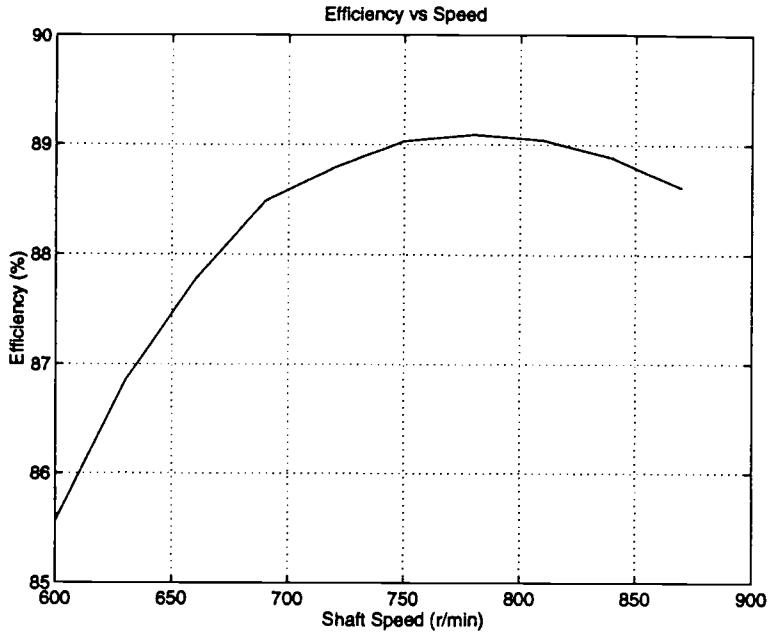

Figure 5.4. "NEMA" Design : Machine Efficiency : Pump Load

Parameter	Square Pole Machine	NEMA Frame Machine
Rotor		
Length	11cm (4.3")	16.5cm (6.5")
Diameter	20cm (8")	16.5cm (6.5")
Stator		
Diameter	38cm (15")	30cm (12")
Back Iron	7cm (2.8")	5cm (2")
Slot Height	2cm (0.8")	2cm (0.8")
Frame Size	22 x 40cm (8.6"x16")	27 x 32cm (10.5"x13")
NEMA Frame	324T	256T

Table 2. Comparison of Two 5hp Design Dimensions

Stack Diameter	$30cm$	Stack Length	$16.5cm$
Slots	36	Slot Pitch	10°
Slot+Tooth Width	$1.31cm$	Slot Depth	$2cm$
Slot Shape	Trapezoidal	Slot Width	$0.64cm \rightarrow 0.80cm$
$\frac{Slots}{pole*phase}$		Winding Pitch	
Power	2	Power	150°
Control	6	Control	120°
$\frac{turns}{coil}$			
Power	12	Back Iron Depth	$4cm$
Control	14		

Table 3. Proposed Design Stator Description

256T, which would house a $7.5hp$, $900\frac{r}{min}$ induction machine, leading to a derating of frame size.

While the square pole approach theoretically provides better performance than the "NEMA-frame" approach, for this design, the main goal is to demonstrate the viability of BDFM technology to as broad an audience as possible, so the "NEMA-frame" machine is proposed. Since this drive will be compared to induction machine drives of similar size, the size of the motor should be as close as possible to a comparably rated induction machine.

5.2 Stator Design

The stator design is summarized in Table 3. The 5hp BDFM is specified to have a DC-point at $900\frac{r}{min}$, so according to Equation 2.1, 3 pole-pairs on the power winding and 1 pole-pair on the control winding are required. The number of stator slots must be factorable by both 18 and 6. As a compromise between harmonic content and tooth width, 36 slots were chosen, giving 2 slots per pole per phase on

the power winding. The amount of space at the airgap into which both the tooth and slot must fit is $1.31cm$.

The number of $\frac{turns}{coil}$ on the power winding was selected to minimize the converter rating and "optimize" the machine performance. 12 $\frac{turns}{coil}$ on the power winding gave a near-minimum converter size and a minimum back iron depth, while 10 $\frac{turns}{coil}$ gave a higher converter size and larger back iron and 14 $\frac{turns}{coil}$ gave a slightly lower converter rating but increased back iron.

The number of $\frac{turns}{coil}$ on the control winding was selected such that the control winding voltage never exceeded $230V_{ll}$ during any of the proposed operating points. One of the requirements of the machine is to operate in a controlled manner down to $100\frac{r}{min}$, to demonstrate the speed control of the rotor. With 14 $\frac{turns}{coil}$ on the control windings and no conditions on the power winding power factor, the required control winding excitation is $100V_{ll}$. At $600\frac{r}{min}$ and rated torque, the required control winding excitation for unity power factor on the power winding is $200V_{ll}$.

The airgap was sized to reduce machine flux densities and allow the machine to fit into a smaller frame. Originally, the airgap was specified at $0.4mm$, resulting in control converter of only 1kVA, but unmanageable back iron flux densities. The airgap was increased to $0.8mm$, increasing the control converter size to 1.6kVA, but reducing flux densities to manageable levels.

Figure 5.5 shows a "snap-shot" of tooth flux densities in the motor at $900\frac{r}{min}$ and 5hp. With steel typically saturating at $1.5 - 1.7T$, a small fraction of the teeth in the motor could be in saturation due to the summation of the 2-pole and 6-pole windings. The power and control winding MMFs are rotating at different frequencies, so "beat-saturation" will occur when the peaks of the control and power tooth fluxes sum in a tooth. Overall, the effect of the momentary saturation will likely be quite small.

5.3 Rotor Design

To provide the best utilization of the aluminum rotor bars and minimize the

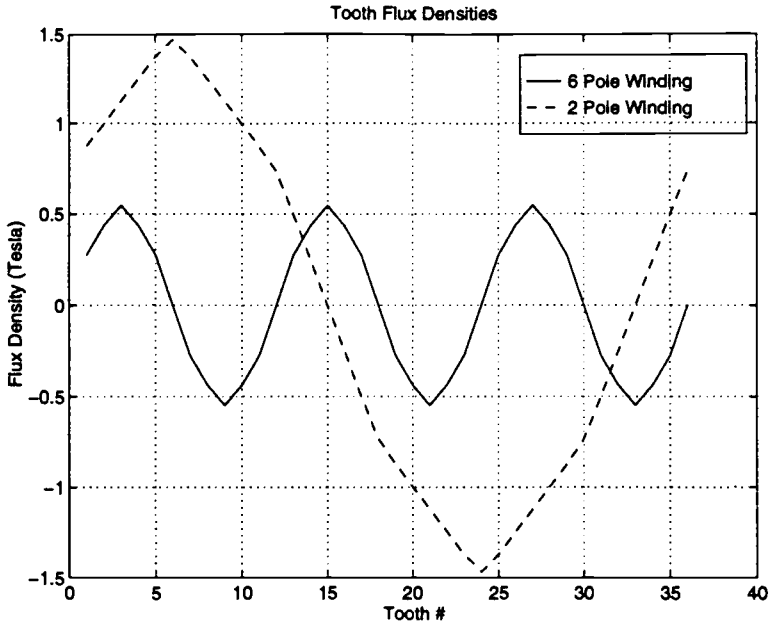

Figure 5.5. Stator Tooth Flux Densities

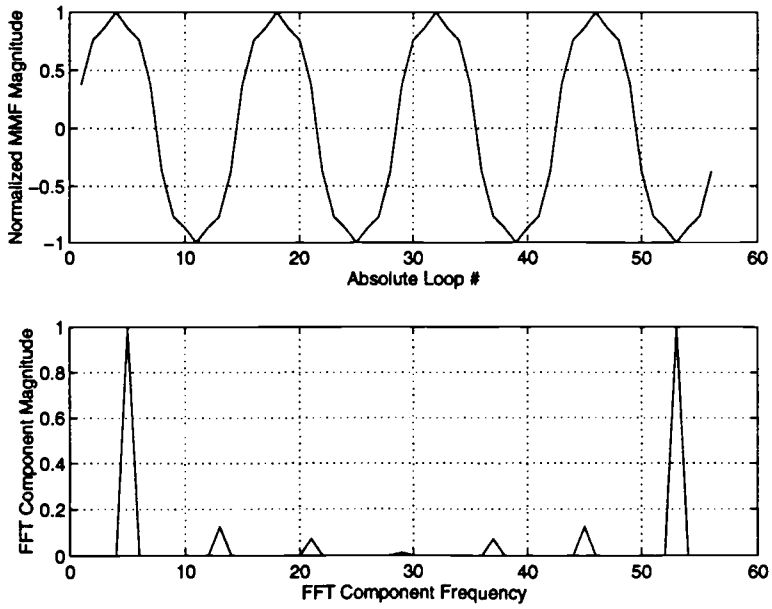

Figure 5.6. Rotor Current Induced MMF for $3\frac{Loops}{Nest}$

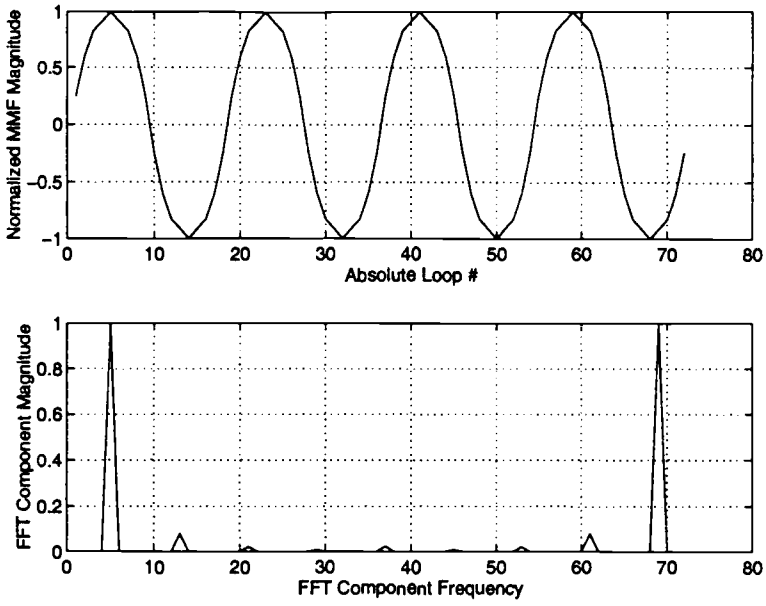

Figure 5.7. Rotor Current Induced MMF for $4\frac{Loops}{Nest}$

potential effect of interbar voltages, a caged rotor is used. Due to the large currents and the phase of the voltage induced on the outer loops, the voltage differential between the two non-caged outer loops is of the order of a few volts. Given the difficulty in die-casting consistently and producing fully isolated loops, a few volts could cause large asymmetrical currents to flow in the rotor steel.

The "NEMA-Frame" design was tried with 3 and 4 bars per nest. The harmonic contents on the spatial MMF due to the rotor currents are shown in Figures 5.6 & 5.7. The harmonic content of the MMF was calculated using the predicted rotor current distribution and the fft function in Matlab. *absolute loop number* refers to the sequential numbering of loops around the rotor without consideration of nest boundaries. Note that in the Figures, there are twice as many *absolute loops* as actual loops on the rotor. This was done to increase the accuracy of the fft function by supplying it with more points. Also note that because the fft is digital, it is symmetrical about the midpoint. The 4 bars per nest design resulted in lower harmonic content and provided enough interbar space to keep the flux-density manageable, so

Rotor Configuration	Caged
Nests	4
$\frac{Loops}{Nest}$	4
Bar-Bar Width	$1.85cm$
Bar-Bar Spacing	Equidistant
Bar Material	Aluminum

Table 4. Proposed Design Rotor Description

4 bars per nest were used for the design.

A diagram of the rotor bar structure and sizings is shown in Figure 5.9.

An overview of the rotor design is provided by Table 4.

Figure 5.8 shows the current distribution in rotor bars for a pump torque characteristic across the 600 to $900\frac{r}{min}$ speed range. As the rotor speed decreases, the currents in all bars decrease to below the $900\frac{r}{min}$ case levels, so rotor bars can be designed for the $900\frac{r}{min}$ case without fear of over-heating the small bars at lower rotor speeds.

The rotor bar currents and the proposed rotor bar dimensions for 5hp at $900\frac{r}{min}$ operation are shown in Table 5.3. The rotor bar current distribution was generated using the MLM. A current density of $2.4\frac{A}{mm^2}$ was assumed for the calculation of bar area. This value was derived from the commonly used stator coil current density for copper of $3.8\frac{A}{mm^2}$, by scaling the current density down by the ratio of copper resistivity to aluminum resistivity.

The rotor bars are very deep and initially concerns were raised about the effect of the skin effect on the bar resistance. At $50Hz$, skin depth is $11mm$, giving a maximum dimension of $22mm$. At $600\frac{r}{min}$, the frequency of the rotor currents is $20Hz$, for a skin depth of $17mm$ and a maximum dimension of $34mm$. Skin effect should not pose a problem with the large bars in this machine, due to the low

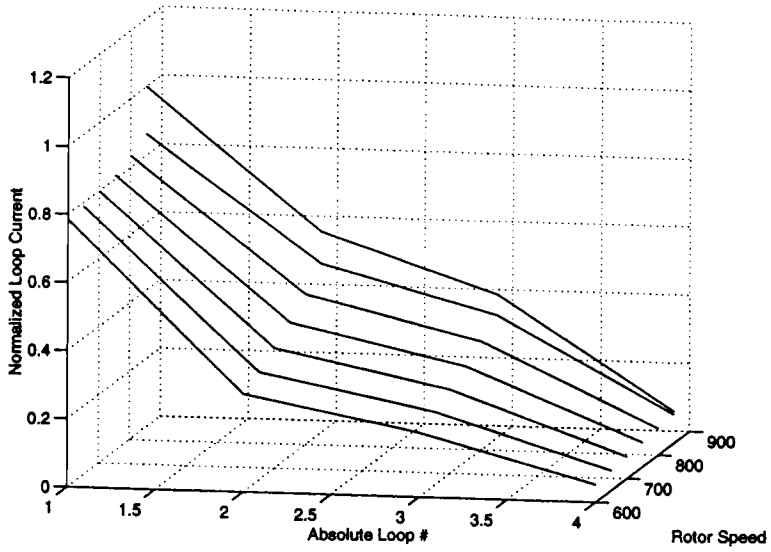

Figure 5.8. Rotor Currents : $600 \rightarrow 900 \frac{r}{min}$: Pump Load

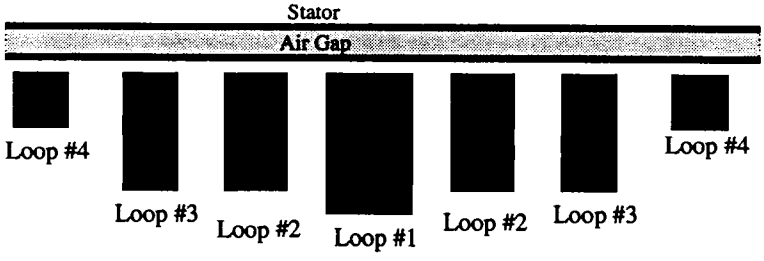

Figure 5.9. Rotor Bar Diagram

	Bar Number			
	1	2	3	4
Current(A)	470	290	250	90
Needed Bar Area (mm^2)	195	121	105	46
Actual Bar Dimension $(mm)(WxD)$	$11x18$	$8x15$	$7x15$	$7x7$

Table 5. Current Distributions in Rotor Bars and Bar Sizes at $900\frac{r}{min}$

electrical frequencies present in the rotor.

5.4 Cost Estimate

Table 5.4 compares the cost estimates of similarly rated BDFM and induction machine drives [15]. The cost of a BDFM was based on the cost of a 6.25hp induction machine. The cost difference between a BDFM and an induction machine system is small due to the considerable number of common, fixed cost items (*e.g.* microcontroller, case) which make up a large percentage of a small converters cost. For example, a 5hp converter is 34% more expensive than a 2hp converter, while a 50hp converter is 121% more expensive than a 20hp converter.

The BDFM ASD system is also more energy efficient than a comparable induction machine ASD. Assuming a converter efficiency of 90% and an 80% 8-pole induction machine [15], system efficiency for the BDFM ASD system at unity power factor on the power winding and 5hp output at $900\frac{r}{min}$ is 85%, while the induction machine efficiency is 72%. This discrepancy is due to converter only feeding a small percentage of power to the BDFM, thereby reducing the effect of the converter efficiency drop on system efficiency.

While this comparison is imperfect, *e.g.* the induction machine drive can operate with a uni-directional converter input, while the BDFM requires a bi-directional

$5Hp$ Induction Machine Drive		$5Hp$ BDFM Drive	
Part	Cost	Part	Cost
$900\frac{r}{min}$, 5hp Induction Machine	\$1,554	5hp BDFM	\$1,721
5hp Drive	\$1,339	2hp Drive	\$994
5hp Line Reactor	\$284	2hp Line Reactor	\$206
Total :	\$3,177	Total :	\$2,921

Table 6. Cost Estimate

converter input, the comparison does demonstrate that the BDFM has potential as a low cost induction machine alternative. Further, the cost comparison would greatly favor the BDFM if efficiency and cost-of-operation are taken into account.

Chapter 6
200kW Stand-alone Aircraft Generator

For this design, a potential client is interested in exploring the use of the BDFM for on-board aircraft, stand-alone power generation. This project was started as a feasibility study to see if the BDFM could be applied to aircraft power generation. To leave as much flexibility as possible, the client's specifications for the design, shown in Table 6, are very general. No size specifications were given.

6.1 Summary of Aircraft Power Generation

Presently, synchronous machines are used for aircraft power generators. Synchronous machines, while not as reliable or maintenance-free as induction machines, have a field winding to control output power factor. The field winding also serves a fault-tolerant purpose: if a short occurs at the 3-phase output, the field is still generated by the field windings, enabling sufficient current to cause breakers to open. When the fault is cleared, output voltage returns to normal. In an induction machine generator, if a fault shorts the output windings, the MMF collapses; when the fault is cleared, there is nothing to restore the MMF, unless some external source is available, and the generator does not resume operation.

The 3-phase output of the synchronous machine is fed to a 300kVA ac-ac converter which then outputs the $400Hz$, $460V_{ll}$ power for the aircraft's power systems. Further, the field winding is powered by a converter which is generally rated at about 10% of the machine rating, or $30kW$. The total system would be comprised of a synchronous machine, which is about 25% larger than a similarly rated induction machine, and two separate converters at $300kVA$ and $30kW$.

Synchronous machines have brushes to contact the rotor and provide power for the field winding. Brushes need to be cleaned to remove dirt and corrosion and

Parameter	Specification
Rotor Speed	$12,000 \rightarrow 24,000$ RPM
Power Output	$200kW@460V_{ll}$
Power Output Frequency	$400 \pm 10\% Hz$
Power Factor	0.7 lagging
kVA Output	$300kVA$
Winding Current Density	$23\frac{A}{mm^2}$
Maximum Flux Density	2.33 Teslas

Table 7. Specification for Aircraft Power Generation System

are another source of potential mechanical failure or a source of airborne conductive dust. The extra down-time of the aircraft due to sychronous machine maintenance could be avoided if induction-type machines could be used instead.

Permanent magnet(PM) machines, which are attracting attention due to their small size, could also be used for power generation on aircraft. As with the synchronous machine, the PM machine has a field located on the rotor and would be able to clear faults on the bus. Whereas a synchronous machine requires a field winding and a converter to power the field, the PM machine has permanent magnets to generate the field and requires no field winding. As with the induction machine, the permanent magnet machine has no brushes contacting the rotor and its reliability should be high, were it not for the poor mechanical properties of permanent magnetic materials. The PM machine could have problems with high-speed operation due to the magnets corrupting the rotor's structural integrity. The PM machine output frequency is directly proportional to the rotor mechanical frequency, so a 300kVA ac-ac converter is needed to convert the PM machine output to $400Hz$. Further, the output voltage of a PM machine is proportional to the rotor speed, so, for the speed-range given, the converter would need to operate from full-input voltage down to half

Parameter	3-1 Machine	4-2 Frame Machine
Rotor		
Length	23cm (9")	18cm (6.5")
Diameter	40cm (15.7")	43cm (17")
Stator		
Diameter	90cm (35.4")	81cm (31.9")
Back Iron	23cm (9.1")	17cm (6.7")
Slot Height	2cm (0.8")	2cm (0.8")
Slot Width	.5cm (0.2")	.3cm (0.12")
Frame Size	90 x 40cm (35.4"x15.7")	81 x 32cm (10.5"x13")

Table 8. Comparison of Two $200kW$ Design Dimensions

input voltage, depending on speed. With this restriction, the converter needs to be rated at full voltage and *double* the full input current, due to low speed voltage. PM machines are more expensive than induction, synchronous, or brushless doubly-fed machines due to the cost of the permanent magnet material.

The above generator solutions require that all the power be processed by a power converter, so a gearbox might not be necessary to lower the generator output frequency.

6.2 BDFM Design Alternatives

Two designs were tried for this project: a 3-1 and a 4-2 BDFM. Comparisons of the two designs are shown in Tables 8 and 9. Figures 6.1 and 6.2 show the converter requirements for the two machines.

With $400Hz$ on the power winding, the natural speeds for 3-1 and 4-2 BDFMs are 6000 and $4000\frac{r}{min}$, respectively. The high speed of the engine dictates that a gearbox be used to couple the BDFM to the engine. The gearbox size is determined

Parameter	3-1 Machine	4-2 Machine
Speed Range	$4250 \rightarrow 8500 \frac{r}{min}$	$2800 \rightarrow 5600 \frac{r}{min}$
Converter Rating	200kVA	200kVA
Efficiency	89%	89%
Air Gap	$1.7mm$	$2mm$

Table 9. Comparison of Two 200kW Design Performances

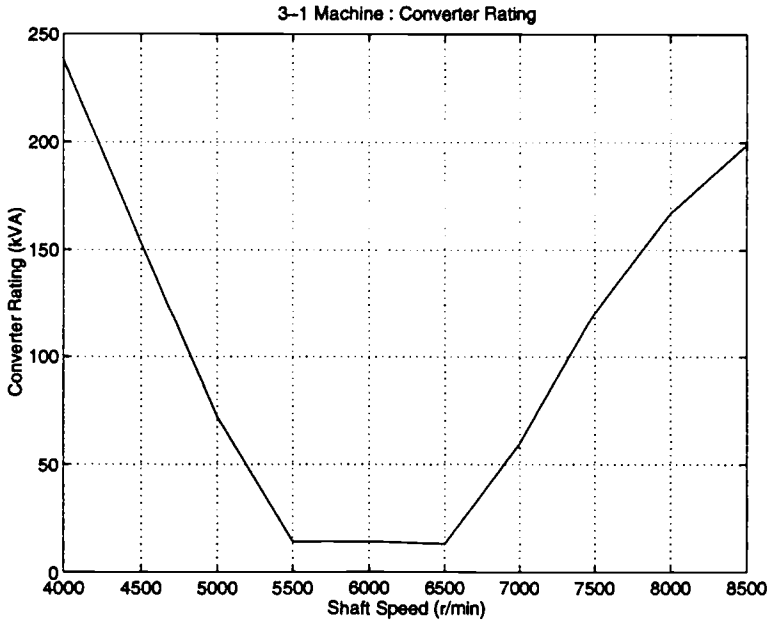

Figure 6.1. 3-1 Machine : Converter Rating

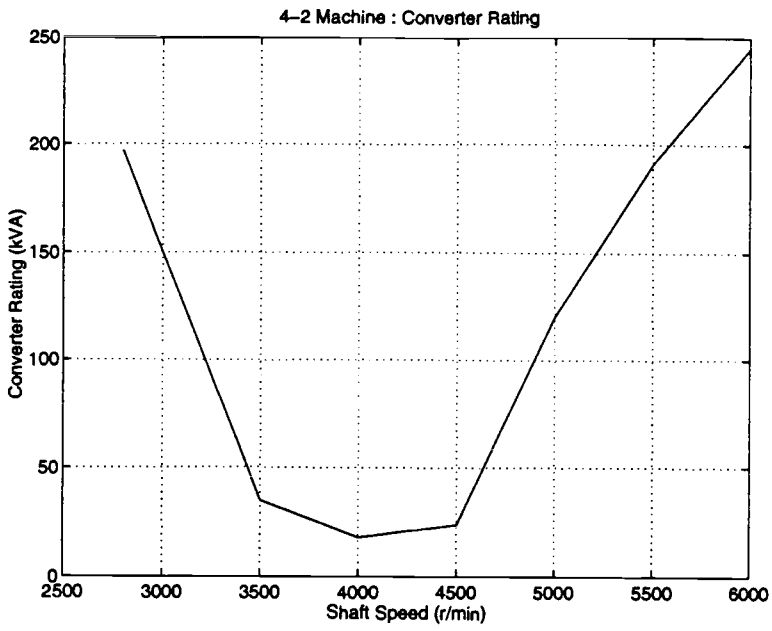

Figure 6.2. 4-2 Machine : Converter Rating

such that the synchronous speed of the BDFM falls just above the operating speed range of the generator system. The synchronous speeds for the 3-1 and 4-2 BDFMs are 8000 and $6000\frac{r}{min}$, respectively, giving gear ratios of 3:1 and 4:1, respectively.

The requirement to drive a load with a lagging 0.7 power factor requires that the BDFM generator be overexcited to generate positive VARs. This increases the converter size, because the converter supplies some of the VARs through the control winding. The converter rectifier side is bi-directional, so it is used to supply some VARs to ease the over-excitation requirements for the power winding.

The power winding output frequency is allowed to vary around 400Hz by $\pm 10\%$ to reduce the converter rating.

Two unusual design specifications were given : the steel can be used up to 2.33 Teslas without saturation and stator current densities of $23\frac{A}{mm^2}$ are allowable. In aircraft, space is at a premium, so very high-grade, high cost steel is used to minimize the machine size. To reduce the motor size further, liquid cooling is used and extremely high current densities can be achieved.

6.3 Proposed Design

A BDFM stand-alone system uses power extracted from the power winding to drive the control winding. As the machine would be required to be a starter motor for the aircraft turbine, startup power requirements would be supplied by the terminal. Short-circuit capabilities were not investigated for this design.

Operating above the natural speed of the machine, a BDFM generator generates power from both the power and control windings, giving a smaller machine for a given power level. Below the natural speed, the control winding takes power from the power winding, necessitating a larger machine to drive both the grid and the control winding.

Running at the lowest speed of $4000\frac{r}{min}$, the 3-1 machine is 33% below the natural speed. The 4-2 machine is 25% below the natural speed at the lowest speed of $3000\frac{r}{min}$.

The size of the back-iron on a BDFM is largely dependent on the number of poles on the control winding. With only one pole pair, the back iron is $23cm$ deep. With two pole pairs, the back iron is $17cm$ deep. In both cases, the back iron flux density is set to $2.3T$.

The back iron was sized to keep the back iron flux densities just above $2.2T$. Peak back iron flux densities in both designs were about $2.3T$.

The tooth flux density for the 4-2 BDFM is shown in Figure 6.4. The peak tooth flux densities, due to power and control windings respectively, are $0.8T$ and $1.8T$. The steel used in aircraft generators begins to saturate at $2.2T$, so a small fraction of the teeth could be in saturation, depending on the angle between the power and control winding fields. In the 3-1 machine, the tooth flux densities, shown in Figure 6.3, peak at $1.1T$ and $2.9T$, saturating a comparatively large number of stator teeth and significantly increasing the harmonic content of the power winding current. To reduce this saturation for the 3-1 machine would require a large increase in the machine diameter, to provide a larger tooth width.

The 4-2 machine is proposed for use as the stand-alone aircraft generator based

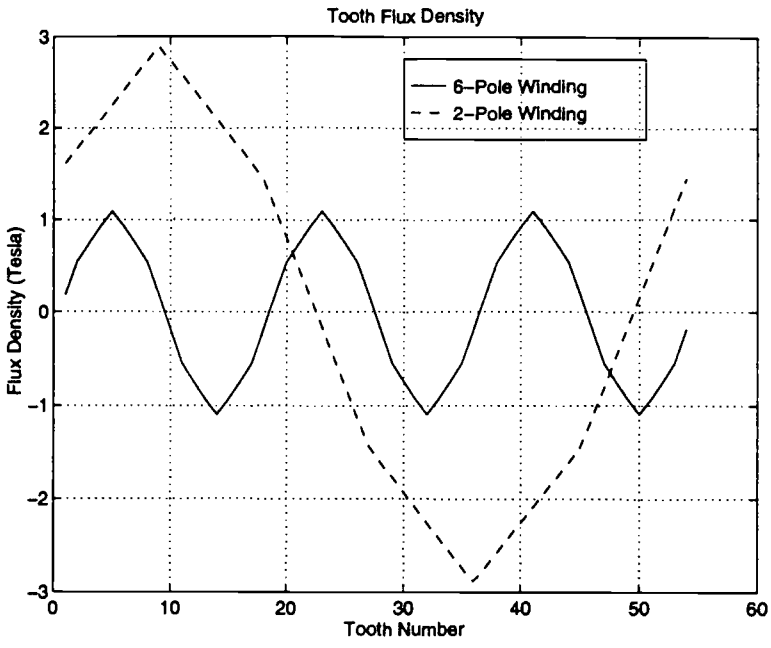

Figure 6.3. 3-1 BDFM Design Tooth Flux Densities

on converter size and the overall machine size and weight, which are crucial in aircraft applications.

The rotor bar design is summarized in Table 6.3. Rotor bars are spaced equidistantly. For this rotor design, the allowable current density is higher due to the oil cooling used in aircraft generators. While the specification allows stator current densities of $22\frac{A}{mm^2}$, the rotor current density was set at $5\frac{A}{mm^2}$ to reduce losses in the rotor bars.

As in the 5hp design, the skin effect should not effect the rotor bars. The maximum electrical frequency on the rotor is 50Hz, giving a maximum dimension of $22mm$.

6.4 Cost Estimate

Table 6.4 compares the cost estimates of similarly rated BDFM and induction machine stand-alone generator systems [15]. The cost of a BDFM was based on the

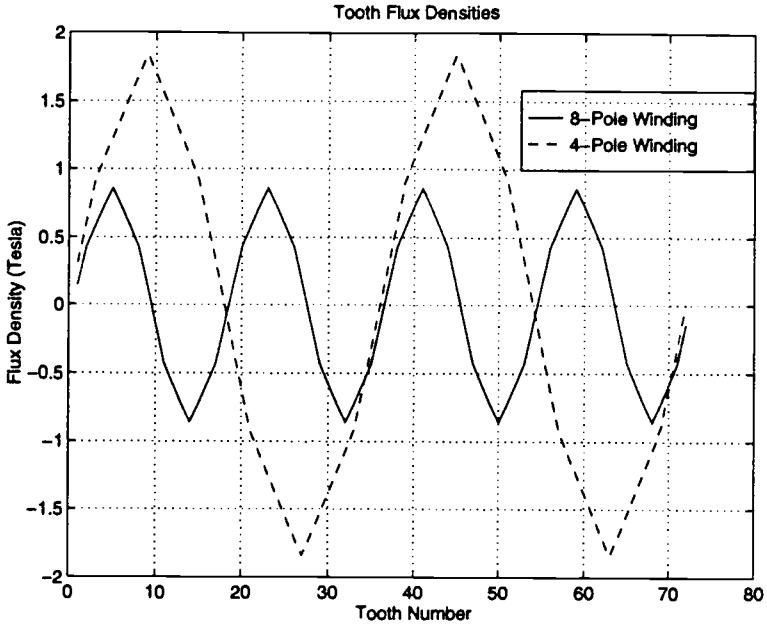

Figure 6.4. 4-2 BDFM Design Tooth Flux Densities

	Bar Number			
	1	2	3	4
Current(A)	2800	2100	2100	500
Required Bar Area (mm^2)	580	420	420	100
Actual Bar Dimension $(mm)(WxD)$	$24x25$	$16x25$	$16x25$	$10x10$

Table 10. Current Distributions in Rotor Bars and Bar Sizes

$300Hp$ Induction Machine Drive		$300Hp$ BDFM Drive	
Part	Cost	Part	Cost
4 Pole 300hp Induction Machine	\$11,000	350hp BDFM	\$16,000
300hp Drive	\$39,600	200hp Drive	\$28,200
300hp Line Reactor	\$1,900	200hp Line Reactor	\$1,600
Total	\$52,500	Total	\$45,800

Table 11. Cost Estimate

cost of a 350hp induction machine. While the comparison is by no means perfect (this comparison assumes 60Hz, while the aircraft power is 400Hz), the reasonable conclusion is that the BDFM system is significantly less expensive than the induction machine alternative.

A synchronous machine system, presently used in aircraft power generation, would cost more than an induction machine drive, due to the increased complexity and size of the synchronous machine and the increased converter cost due to the field winding.

Chapter 7
Design Conclusion

The MLM appears to predict with reasonable accuracy the current distributions among the rotor bars. With knowledge of the current carried in each bar, the bars can be sized accordingly.

Theoretically, the square pole design approach will give the best performance. This approach uses the least wire to achieve the same mutual inductance, lowering resistance and leakage inductance. The square pole approach also results in a wide, thin rotor, which gives extra room in the stator for the slots. This extra room allows for extra copper to be used and for wider slots.

Practically, the low cost of induction machines does not allow custom frames to be used for small to medium power applications. Most small induction machines are constructed using NEMA frames, but the aspect ratios of NEMA frames disallows the use of the square pole design approach for BDFM construction. Large machines, where it becomes practical to use custom frames, could use the square pole design approach.

The design of the 5hp BDFM shows that cheap, readily available NEMA induction machine frames are practical to use for BDFMs. The efficiency of the BDFM is comparable to "premium-efficiency" 5hp, 6-pole induction machines and higher than 5hp, 8-pole induction machines. System efficiency for the proposed 5hp BDFM is significantly higher than the theoretical efficiency of either 6-pole or 8-pole induction machine drives.

The design of the $200kW$ BDFM demonstrates that the BDFM is applicable to stand-alone power generation in aircraft. Since no dimension specifications were given for the aircraft generator, the square pole design approach was used to design both the 3-1 and 4-2 machine. The converter for this application is rated at 60% of the machine rating, providing a significant cost and space reduction.

In both the 5hp and the $200kW$ designs, tooth flux density proved to be a major design problem. The control winding's lower pole-pair number results in high flux densities. The high back iron flux can be accommodated by increasing the back iron depth. The tooth flux densities are a more challenging problem, due to the relatively fixed size of the stator teeth. The solution to the problem required increasing the airgap. In the 5hp design, increasing the airgap led to decreased magnetizing inductances on the power and control windings, which increased converter requirement, due to the increased need for magnetization of the 6-pole winding by the 2-pole winding, and reduced flux levels, due to the reduced magnetizing inductance. In the $200kW$ design, the increased airgap reduced flux levels, but didn't affect converter rating significantly.

Chapter 8
Conclusions

Adjustable speed drives and variable speed generator systems have become popular in recent years due to their flexibility and potential for process improvement. Inherent in most ASD and VSG systems is the need for power electronics rated to process the full kVA input/output of the system. The high cost of power electronics is driving the search for systems in which the converter size can be minimized. The BDFM is an ASD and VSG system candidate in which the converter size can be a fraction of the machine rating.

Due to the complexity of the BDFM, modelling efforts have not taken into account the special rotor construction or addressed the current distributions in seperate rotor loops. A Multiple Loop Model of the BDFM has been developed and programmed using Matlab. The model is presented herein and it's implementation in Matlab is discussed.

To validate the MLM for use in motor design, the MLM's current predictions are compared to current predictions from a finite element analysis and to current measurements from an experimental laboratory setup in which the individual rotor loop currents are accessible. The MLM's results closely agree with both the finite element analysis and the experimental results, suggesting that the MLM is an accurate and appropriate model upon which to base future BDFM design efforts.

To demonstrate use of the MLM, two machine designs are presented : a 5hp demonstration machine and a 200kW, stand-alone aircraft generator. Both of the designs use the MLM's predictions of loop current distributions to size rotor bar and distribute losses evenly around the rotor.

The 5hp machine is to be used for BDFM demonstration purposes and is designed to show a wide variety of BDFM behavior. Due to the wide range of applications

this machine is designed to demonstrate, it was "optimized" to operate over a wide speed range unloaded, from $600 \rightarrow 900 \frac{r}{min}$ with pump load characteristics and as a high-speed generator.

The 200kW generator design demonstrates that the BDFM is applicable to stand-alone aircraft power generation. The power electronics used to excite the control winding is rated at a fraction of the machine rating, whereas other stand-alone generator systems would require converters scaled, at minimum, to the full machine rating.

With the Multiple Loop Model, future BDFM designs will be able to scale rotor conductors to distribute losses equally around the rotor and minimize rotor conductor usage, reducing rotor cost and allowing for increased inter-bar steel.

BIBLIOGRAPHY

[1] C. Brune, R. Spee, and A.K. Wallace, "Experimental Evaluation of a Variable Speed, Doubly-Fed Wind Power Generation System," in *IEEE Industry Applications Society Annual Meeting Conference Record*, pp. 480–487, 1993.

[2] Y. Xu and Y. Tang, "A Novel Wind Power Generating System Using Field Orientation Controlled Doubly-Fed Brushless Reluctance Machine," in *IEEE Industrial Application Society Annual Meeting Conference Record*, pp. 408–413, 1992.

[3] A. Kusko and C. B. Somuah, "Speed Control of a Single-Frame Casacade Induction Motor with Slip Power Pump Back," *IEEE Transactions on Industry Applications*, vol. IA-14, pp. 97–105, Apr. 1978.

[4] Alan Wallace, Rene Spee, and Hian K. Lauw, "The Potential of Brushless Doubly Fed Machines for Adjustable Speed Drives," in *IEEE Pulp and Paper Industry Technical Conference*, pp. 45–50, 1990.

[5] F. Creedy, "Some Developments in Multi-Speed Cascade Induction Motors," *Journal of the IEE*, vol. 39, pp. 648–667, 1977.

[6] A.R. Broadway and L. Burbridge, "Self-Cascaded Machine: A Low Speed Motor or High-Frequency Alternator," in *IEE Proceedings*, vol. 117(7), pp. 1277–1290, 1970.

[7] R. Li, A.K. Wallace, R. Spee, and Yixin Wang, "Two Axis Model Development of Cage Rotor Brushless Doubly-Fed Machines," *IEEE Transactions on Energy Conversion*, vol. 6(3), pp. 453–460, Sept. 1991.

[8] M.S. Boger, A.K. Wallace, R. Spée, and R. Li, "General Pole Number Model of the Brushless Doubly-Fed Machine," in *IEEE Industrial Application Society Annual Meeting Conference Record*, 1994.

[9] R. Spee, A.K. Wallace, and H.K. Lauw, "Simulation of Brushless Doubly-Fed Drives," in *IEEE Industry Application Society Annual Meeting*, (San Diego), 1989.

[10] R. Li, A.K. Wallace, and R. Spee, "Dynamic Simulation of Cage Rotor Brushless Doubly-Fed Machines," *IEEE Transactions on Energy Conversion*, vol. 6(3), pp. 445–452, Sept. 1991.

[11] B.E. Thompson, "Three-Dimensional Finite-Element Design PRocedure for the Brushless Doubly-Fed Machine," Master's thesis, Oregon State University, Jan. 1995.

[12] A. Kemp, M. Boger, E. Wiedenbrug, and A. Wallace, "Investigation of Rotor-Current Distributions in Brushless Double-Fed Machine," in *IEEE Industry Applications Society Annual Meeting*, (San Diego), 1996. Accepted for Presentation.

[13] Michael S. Boger, "General Pole Number Model of the Brushless Doubly-Fed Machine," Master's thesis, Oregon State University, July 1994.

[14] A.R. Kemp, "Compilation of Multiple Loop Model Programs Relevant to 1996 Master's Thesis," June 1996.

[15] Baldor Motors and Drives, "1994 Stock Products Catalog," 1994.

APPENDIX

BDFM Simulator Programming

Due to the nature of the BDFM, it difficult to develop programs which automate the simulation of BDFM.

For example: increasing the control voltage will usually increase the power factor on the power winding. If the control winding is very over-excited, the program would expect the over-excited power winding to have a capacitive power factor. Due to the model's predictions and the algorithm for finding the "proper" operating point, the power factor on the power winding will return to an inductive power factor. Predicting whether to increase or decrease the control voltage becomes very difficult, because there is no way to figure out if an operating point is legitimate or whether the operating point is a fluke of the model.

The BDFM control winding voltage is highly dependent on the frequency of the control winding excitation. During a simulation, if the next speed point is much different than the previous point, the control winding could over-excite the machine and cause problems as mentioned above. There is no way to predict whether the operating point due to a control voltage is too over-excited or realistic.

A unit change in control voltage does not provide a unit change in power factor, due to the non-linear nature of the power factor. This requires that an interative approach be taken to solve for the control voltage. In the interest of time, the quickest solution is desirable, but due to the breadth of conditions and target operating points, a slower approach is necessary. To increase the perceived linearity of the system for the adjustments of control voltage, a four quadrant tangent is used to convert the power factor to radians. The radians are then a nearly linear function of control voltage.

The above challenges were found during the programming of the BDFM motor simulator. The BDFM stand-alone generator simulator involves the above problems and a few problems due to the closed system.

As mentioned above, power factor is a non-linear function of control voltage. In the stand-alone system, the power factor is a more complex function due to the

interaction of the control and power windings. This requires a more conservative approach to the iterative solution of the control voltage.

The problem of over-excitation of the stand-alone generator system is also aggravated by the interaction of the control and power windings. So far, no solution to predicting whether the machine is over-excited or not has been found. Presently, the programmer is responsible for recognizing the problem and correcting it manually.